

# Chemiosmotic nutrient transport in synthetic cells powered by electrogenic antiport coupled to decarboxylation

Received: 17 April 2024

Accepted: 27 August 2024

Published online: 12 September 2024

 Check for updatesMiyer F. Patiño-Ruiz <sup>1,2</sup>, Zaid Ramdhan Anshari <sup>1,2</sup>, Bauke Gaastra<sup>1</sup>, Dirk J. Slotboom <sup>1</sup> & Bert Poolman <sup>1</sup> 

Cellular homeostasis depends on the supply of metabolic energy in the form of ATP and electrochemical ion gradients. The construction of synthetic cells requires a constant supply of energy to drive membrane transport and metabolism. Here, we provide synthetic cells with long-lasting metabolic energy in the form of an electrochemical proton gradient. Leveraging the L-malate decarboxylation pathway we generate a stable proton gradient and electrical potential in lipid vesicles by electrogenic L-malate/L-lactate exchange coupled to L-malate decarboxylation. By co-reconstitution with the transporters GltP and LacY, the synthetic cells maintain accumulation of L-glutamate and lactose over periods of hours, mimicking nutrient feeding in living cells. We couple the accumulation of lactose to a metabolic network for the generation of intermediates of the glycolytic and pentose phosphate pathways. This study underscores the potential of harnessing a proton motive force via a simple metabolic network, paving the way for the development of more complex synthetic systems.

Living cells require energy to fuel essential biosynthetic processes, to grow and divide, and to maintain homeostasis and an out-of-equilibrium metabolic state. The two main metabolic energy currencies of a cell are ATP and H<sup>+</sup> (or Na<sup>+</sup>) electrochemical gradients; the latter are referred to as proton and sodium motive force (SMF), respectively. A proton motive force (PMF) can be generated by respiration, light-driven electron transfer reactions, or ATP hydrolysis<sup>1,2</sup>. The PMF is composed of a H<sup>+</sup> chemical gradient, ΔpH (typically alkaline inside), and an electrical potential, ΔΨ (typically negative inside):

$$\text{PMF} = \Delta\Psi - 2.303 \frac{RT}{F} \Delta\text{pH} \quad (1)$$

where  $R$ ,  $T$ , and  $F$  correspond to the gas constant, temperature, and Faraday constant, respectively, and  $\Delta\text{pH} = \text{pH}_i - \text{pH}_o$ .

Fermentative bacteria are unable to form a PMF by respiration or photosynthetic reactions, and the PMF can be formed via ATP hydrolysis

by F<sub>1</sub>F<sub>0</sub>-ATPase<sup>3,4</sup>. However, it is also possible to generate a PMF without involvement of high-energy intermediates like ATP, using electrogenic uniport or electrogenic precursor-product exchange in combination with metabolic breakdown of the substrate inside the cell<sup>3,5</sup>. An example is the internal decarboxylation of substrate (precursor), catalyzed by a soluble decarboxylase, coupled to the uptake of precursor and extrusion of product, mediated by a specific transport protein<sup>6</sup>.

Bacteria of the genera *Lactobacillus*, *Lactococcus*, *Leuconostoc*, and *Pedococcus* possess an L-malate decarboxylation pathway, also known as malolactic fermentation, which generates a PMF and counterbalances intracellular acidification<sup>7,8</sup>. In *Lactococcus lactis*, the cytosolic L-malate decarboxylase (malolactic enzyme, MleS) catalyzes the decarboxylation of L-malate to L-lactate plus CO<sub>2</sub>, while a membrane-embedded secondary transporter, MleP, exchanges dianionic L-malate for L-lactate or mono-anionic L-malate for L-lactic acid. The decarboxylation reaction results in an inward gradient for L-malate and an outward gradient for L-lactate, establishing the driving

<sup>1</sup>Department of Biochemistry, Groningen Biomolecular Sciences and Biotechnology Institute, University of Groningen, Nijenborgh 4, 9747 AG Groningen, The Netherlands. <sup>2</sup>These authors contributed equally: Miyer F. Patiño-Ruiz, Zaid Ramdhan Anshari. ✉e-mail: [b.poolman@rug.nl](mailto:b.poolman@rug.nl)

forces for the L-malate/L-lactate exchange<sup>5</sup>. The CO<sub>2</sub> may leave the cell by passive diffusion without affecting pH<sup>7</sup>. Consumption of scalar protons during the decarboxylation reaction leads to an intracellular alkalization and, therefore, generates a ΔpH across the plasma membrane. The gradual decrease in external L-malate and increase in L-lactate can rise the external pH, because the molecules have a different acidity (L-malate: pK<sub>a1</sub> = 3.4, pK<sub>a2</sub> = 5.1; and L-lactate: pK<sub>a</sub> = 3.8)<sup>7,9</sup>, but generally the impact of L-malate decarboxylation will be highest for the internal pH.

The exchange of di-anionic L-malate for L-lactate or mono-anionic L-malate for L-lactic acid is electrogenic and thus generates a membrane potential (ΔΨ, inside negative). Both components of the PMF are generated in different but coupled steps, which is mechanistically very different from how the PMF is generated in respiration or photosynthesis or upon ATP hydrolysis by F<sub>1</sub>F<sub>0</sub>-ATPase. We refer to the combined action of MleP and MleS as the L-malate decarboxylation pathway. The compartmentalization of the L-malate decarboxylation pathway makes it possible to conserve the low amount of free energy from the decarboxylation reaction (−17 to −25 kJ mol<sup>−1</sup>)<sup>6</sup>, chemiosmotically into a PMF<sup>10</sup>. The free energy change of a carboxylation reaction is too small for the synthesis of ATP from ADP plus Pi, but the formed PMF can be used to supply the cell with ATP and fuel other essential functions like the transport of nutrients. The PMF can also facilitate processes like cell division<sup>11</sup>, (membrane) protein insertion/secretion<sup>12</sup> and intercellular communication<sup>13,14</sup>. Various other PMF-generating precursor-product exchange–decarboxylation pathways have been described (oxalate<sup>2−</sup>/formate<sup>−</sup>, citrate<sup>2−</sup>/L-lactate<sup>−</sup>, arginine<sup>+</sup>/agmatine<sup>2+</sup>, ornithine<sup>+</sup>/putrescine<sup>2+</sup>, glutamate<sup>−</sup>/γ-aminobutyrate, histidine/histamine<sup>+</sup>, tyrosine/tyramine<sup>+</sup>, aspartate<sup>−</sup>/alanine)<sup>15–22</sup>.

In this work, we explore the potential of the L-malate decarboxylation pathway for the generation of a PMF in submicrometer-size lipid vesicles. We co-reconstituted the pathway with *Escherichia coli* glutamate transporter GltP<sup>23,24</sup> and lactose transporter LacY<sup>25</sup>, and we show long-lasting transport and high steady-state levels of these solutes. We also demonstrate the utilization of L-malate-dependent lactose accumulation in downstream metabolic reactions. The sustainable energy conversion by the L-malate decarboxylation pathway enables more complex cell-like metabolic functions and sets the foundations for further out-of-equilibrium networks in synthetic cells.

## Results

The L-malate decarboxylation pathway generates a proton motive force by the action of two proteins: the integral membrane L-malate/L-lactate exchanger (MleP) and the soluble, luminal, L-malate decarboxylase (MleS). To guide the reconstitution of this system in lipid vesicles we characterized both proteins. A summary of the data obtained and in literature is presented in Table 1.

## MleP mediates electrogenic L-malate/L-lactate exchange and L-malate uniport

MleP belongs to the 2-hydroxycarboxylate transporter family (2HCT), which function as symporters or exchangers<sup>26</sup>. MleP has been described as a L-malate/L-lactate exchanger<sup>7</sup> with a molecular weight of 47.9 kDa and 9–14 predicted TMS<sup>26,27</sup>. We overexpressed the 10× His-tagged MleP in *L. lactis*, purified the protein via immobilized metal-affinity chromatography (IMAC) and incorporated the protein in lipid vesicles composed of dioleoyl-phospholipids DOPE:DOPG:DOPC 1:1:2 (mol ratio) or *E. coli* polar lipids: egg PC 3:1 (mol ratio). Figure 1a shows that MleP is reconstituted with an efficiency of 51 ± 9% (Supplementary Fig. 1); the double band is assigned to different structural conformations and incomplete denaturation by SDS. We also observe some dimeric MleP, similar to what has been reported for other members of the 2HCT family<sup>26</sup>.

We determined the electrogenic nature of L-malate/L-lactate exchange by solid-supported membrane (SSM)-based electrophysiological measurements (Fig. 1). The net transfer of charge by the exchange of divalent L-malate for monovalent L-lactate is detected as a transient current via the capacitive coupling between the supported membrane and the vesicles<sup>28</sup>. A negative current is observed when external L-lactate (non-activating solution) is replaced with L-malate (activating solution) with L-lactate-loaded MleP-vesicles adsorbed to the supporting membrane (Fig. 1b, c). A positive peak current is obtained when a L-lactate jump is triggered on L-malate-loaded MleP vesicles, because the charge transport is now in the opposite direction (Fig. 1b, c). There is no substantial current when the same solution exchange is performed in liposomes without MleP (empty liposomes) (Fig. 1c). We reduced the possibility of obtaining electrical artifacts from differences in ionic strength between the activating and non-activating solutions by replacing lactate and malate with acetate and sulfate, respectively, which carry the same charge but are not recognized as substrates by MleP. These results confirm the electrogenic character of the L-malate/L-lactate exchange.

We found that MleP reconstituted at a lipid-to-protein (LPR) ratio of 100 was able to exchange L-malate for L-lactate in the chemically defined synthetic lipid mixture DOPE:DOPG:DOPC 1:1:2 (mol ratio), but the activity was 7 times higher in liposomes composed of *E. coli* polar lipids: egg PC 3:1 (Supplementary Table 1, Supplementary Fig. 2). Therefore, we used the *E. coli* polar lipid/egg PC mixture for the majority of the reconstitutions at LPR 100 and further SSM measurements. The amplitude of the peak current (*I<sub>p</sub>*) is proportional to the steady state L-malate/L-lactate exchange activity<sup>29</sup>. The peak current amplitude increases in a hyperbolic manner with the increment in the outside concentration of L-malate or L-lactate, while keeping the internal concentration of L-lactate or L-malate at 30 mM (Fig. 1d and

**Table 1 | Kinetic parameters of MleP, MleS, GltP, and LacY**

	MleP <sup>i</sup>	MleS <sup>v</sup>	GltP <sup>vii</sup>	LacY
<i>K<sub>m</sub><sup>app</sup></i>	L-malate 0.42 ± 0.11 mM ( <i>n</i> = 3) L-lactate 2.9 mM ( <i>n</i> = 2)	L-malate 1.4 ± 0.4 mM ( <i>n</i> = 3) NAD <sup>+</sup> 0.042 mM Mn <sup>2+</sup> 5–10 μM <sup>vi</sup>	L-glutamate 5.5 ± 0.8 μM	D-lactose 0.5 mM <sup>viii</sup>
pH <sub>opt</sub>	6 <sup>ii</sup>	6	6	8.5–9 <sup>k</sup>
<i>I<sub>max</sub></i> or <i>V<sub>max</sub></i>	−21 ± 5 nA ( <i>n</i> = 5) <sup>iii</sup>	257 ± 13 μmol H <sup>+</sup> min <sup>−1</sup> mg <sup>−1</sup> ( <i>n</i> = 3)	115 nmol L-glutamate min <sup>−1</sup> mg <sup>−1</sup>	35 μmol lactose min <sup>−1</sup> mg <sup>−1</sup> <sup>viii</sup>
Turnover or <i>k<sub>cat</sub></i> (s <sup>−1</sup> )	≈25 <sup>iv</sup>	266 ± 14 ( <i>n</i> = 3)	≈0.1	16–21 <sup>viii</sup>

<sup>i</sup>Electrogenic L-malate/L-lactate exchange was measured in vesicles composed of *E. coli* polar lipids:egg PC 3:1 lipids at lipid-to-MleP ratio of 100 (w/w) for L-malate and L-lactate dependence (pH 7 and 250 (w/w) for pH dependence, using SSM-based electrophysiological measurements at room temperature (Fig. 1). <sup>ii</sup>pH at which the highest peak current amplitude was obtained for the L-malate jump in L-lactate-loaded MleP vesicles in the pH range 6–8.5. <sup>iii</sup>Peak current amplitude for the L-malate concentration jump in L-lactate-loaded MleP vesicles at pH 7 (Fig. 1b, c). <sup>iv</sup>Assumptions made for the estimation of the turnover: (1) The area of the SSM sensor chip (3 mm diameter) is completely covered by one layer of large-unilamellar vesicles with a diameter of 200 nm containing MleP. (2) 50% reconstitution efficiency of MleP (Supplementary Fig. 1). (3) The amplitude of the peak current represents steady-state charge transfer across the membrane. <sup>v</sup>The activity of MleS at pH 7 was measured in low concentration of K-phosphate buffer at 30 °C using a pH microelectrode (Fig. 2). <sup>vi</sup>Taken from<sup>30,31</sup>. <sup>vii</sup>Kinetic parameters obtained from PMF-driven influx in proteoliposomes at 30 °C (pH<sub>o</sub> 5.5, pH<sub>i</sub> 7.5), taken from<sup>24</sup>. <sup>viii</sup>ΔΨ-driven influx in proteoliposomes at pH 7.5 and 25 °C, taken from ref. 42. <sup>ix</sup>SSM-based measurements, taken from ref. 92. Parameters obtained in this study are indicated as mean ± SD from *n* different preparations.

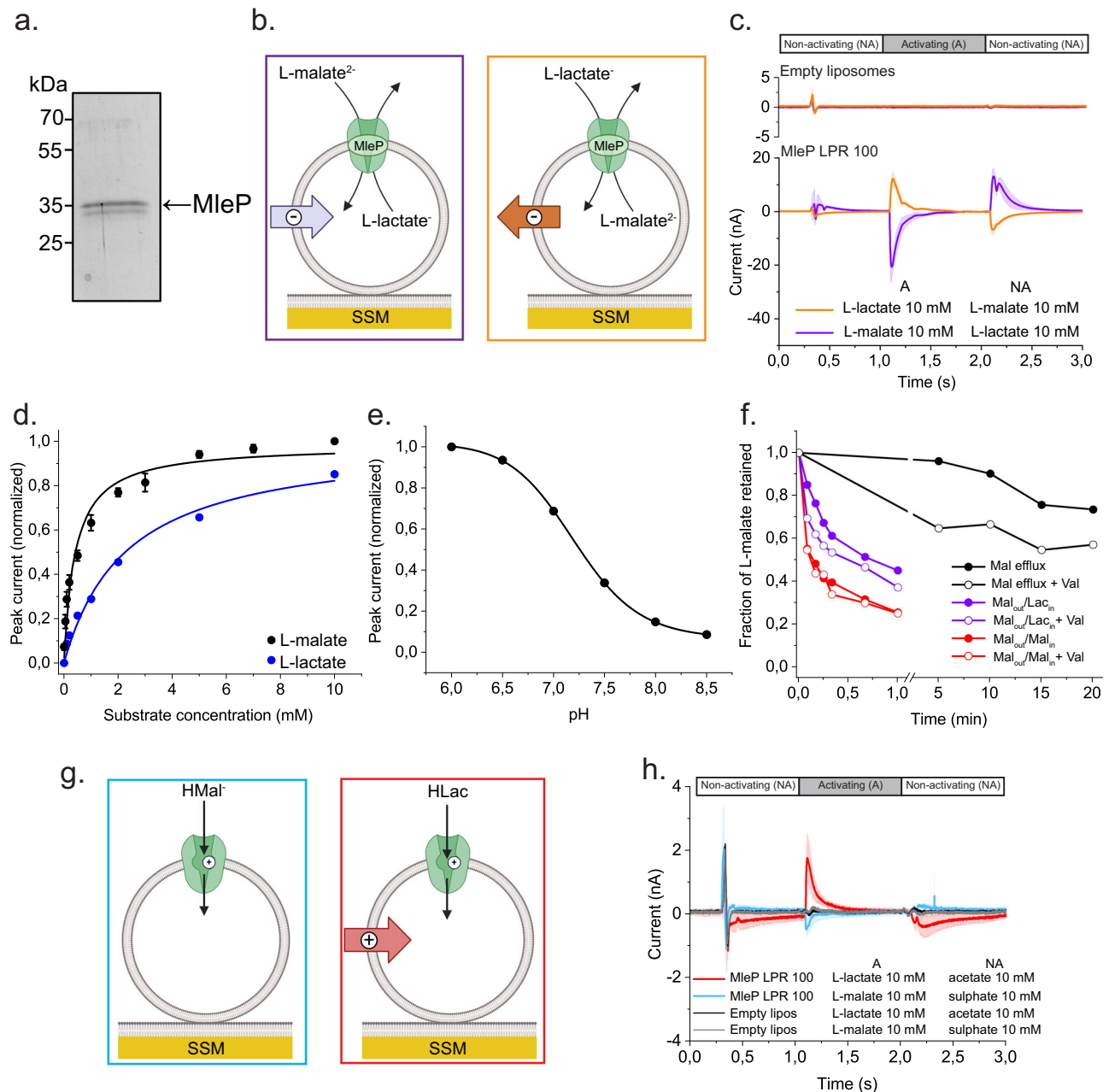


**Fig. 1 | Electrogenic transport activity of MleP.** **a** SDS-polyacrylamide gel of MleP in *E. coli* polar lipids:egg PC 3:1 (mol ratio). (Uncropped gel in Supplementary Fig. 1a). **b** Cartoon of MleP-liposomes loaded onto SSM, indicating the direction of charge transfer during the L-malate<sub>influx</sub>/L-lactate<sub>efflux</sub> (violet box) and L-lactate<sub>influx</sub>/L-malate<sub>efflux</sub> exchange (orange box). **c** Current traces recorded by SSM-based electrophysiology of MleP LPR 100 proteoliposomes ( $n = 3$ ) or empty liposomes ( $n = 2$ ) for L-malate<sub>influx</sub>/L-lactate<sub>efflux</sub> (violet, L-malate jump) and exchange in the opposite direction (orange, L-lactate jump). **d** Normalized peak currents obtained from ON signals for different concentrations of L-malate (black,  $n = 3$ ) and L-lactate (blue,  $n = 2$ ) jumps on L-lactate- and L-malate-loaded MleP liposomes, respectively. Data of peak currents represent the mean from independent experiments with  $n$  different preparations of proteoliposomes. Error bars represent  $\pm$  SD. Solid lines correspond to a Michaelis-Menten fit (black  $R^2 = 0.971$ , blue  $R^2 = 0.985$ ). **e** pH dependence of peak currents obtained from L-malate jumps at the indicated external pHs on MleP LPR 250 liposomes loaded with L-lactate at

pH 7. Data are normalized to the value at pH 6 and correspond to the average from  $n$  independent experiments with different preparations of proteoliposomes ( $n = 2$ ). Solid line represents a sigmoidal function fit of the data ( $R^2 = 0.999$ ). **f**  $^{14}\text{C}$ -L-malate efflux measurements performed on MleP-liposomes (LPR 200 in DOPE:-DOPG:DOPC 1:1:2 (mol ratio)) diluted in buffer containing L-lactate (violet, exchange Mal<sub>out</sub>/Lac<sub>in</sub>), L-malate (red, homologous exchange Mal<sub>out</sub>/Mal<sub>in</sub>) or without counter substrate (black, Mal efflux). Val indicates valinomycin addition and the generation of a  $-100$  mV  $\text{K}^+$  diffusion potential. **g** Cartoon of half turnover transport in MleP-liposomes. **h** Current traces recorded upon a L-malate (blue,  $n = 3$ ) or L-lactate (red,  $n = 3$ ) jump on MleP LPR 100 or empty liposomes loaded with sulfate or acetate, respectively. Current traces in **c**, **h** are presented as the average from independent experiments with different preteoliposome preparations and different SSM sensor chips. Shaded areas =  $\pm$  SD. Mal = L-malate, Lac = L-lactate. **b**, **g** were created with Biorender.com released under a Creative Commons Attribution-NonCommercial-NoDerivs 4.0 International license.

Supplementary Fig. 3a–c). We find that the  $K_m^{\text{app}}$  for L-lactate is 7-fold higher than for L-malate (Table 1 and Fig. 1d).

Since the L-malate decarboxylation leads to an internal as well as external pH change, (see Introduction and<sup>7</sup>), we performed L-malate

jumps on L-lactate-loaded vesicles at pH values between 6 and 8.5 (Supplementary Fig. 3d). Here, we used MleP LPR 250 vesicles to have a similar number of transporters per vesicle as in the experiments with the L-malate decarboxylation pathway. The L-malate/L-lactate activity

is highest at pH 6 and decreased at more alkaline pHs (Fig. 1e). The pH dependence most likely reflects the activity of MleP and not the availability of substrate, because the change in concentration of dianionic L-malate is only 4% between pH 6 and pH 8.5. Besides L-malate/L-lactate exchange, MleP facilitates uniport of L-malate<sup>27</sup>, which would also be electrogenic and enable L-malate decarboxylation because L-lactate can leave the vesicles in the protonated form (L-lactic acid) by passive diffusion. Indeed, transport assays with vesicles loaded with radiolabelled L-malate (Fig. 1f) show efflux of L-malate but with a rate at least one-order of magnitude slower than L-malate/L-lactate exchange. The electrogenic nature of both the uniport and exchange is shown by the increase of activity in the presence of the K<sup>+</sup> ionophore valinomycin, which dissipates the membrane potential. Thus, two different methodologies (SSM-based electrophysiology and efflux of radiolabelled substrate) confirm that MleP is an electrogenic secondary antiporter/uniporter.

The slow kinetics of the uniport reaction complicates the SSM measurements, but we recorded small peak currents when L-malate or L-lactate jumps were applied on MleP vesicles without counter-substrate (Fig. 1g, h). These peak currents can be interpreted as pre-steady state currents that originate from a half turnover, *i.e.* L-malate or L-lactate influx, which is followed by a slow return of the empty

carrier. Interestingly, the peak current from the L-lactate jump is not only 5-fold larger in magnitude but also has a positive direction, indicative of movement of positive charge in or negative charge out of the vesicles.

### L-malate decarboxylation catalyzed by MleS

L-malate decarboxylase MleS catalyzes the decarboxylation of L-malate to L-lactate, releasing carbon dioxide and consuming a proton (Fig. 2a). Protons are used to compensate for the free electron pair remaining in the organic intermediate after the heterolytic cleavage that releases CO<sub>2</sub> (Supplementary Fig. 4)<sup>6</sup>. MleS is a homodimeric protein with a molecular weight of 60–65 kDa per subunit and has NAD<sup>+</sup> and Mn<sup>2+</sup> as bound cofactors<sup>30–32</sup>. The decarboxylation reaction proceeds in three consecutive steps without detectable accumulation of intermediates: (i) L-malate oxidation to oxaloacetate; (ii) decarboxylation of oxaloacetate to pyruvate; and (iii) pyruvate reduction to L-lactate (Supplementary Fig. 4)<sup>26</sup>. The NAD<sup>+</sup> consumed in the first step is recycled in the third step. The proton consumption leads to alkalinization of the cytoplasm.

We overexpressed *L. lactis* MleS and purified the protein by IMAC and size-exclusion chromatography (SEC). A single and symmetrical peak in the SEC and SDS-polyacrylamide gel confirms the

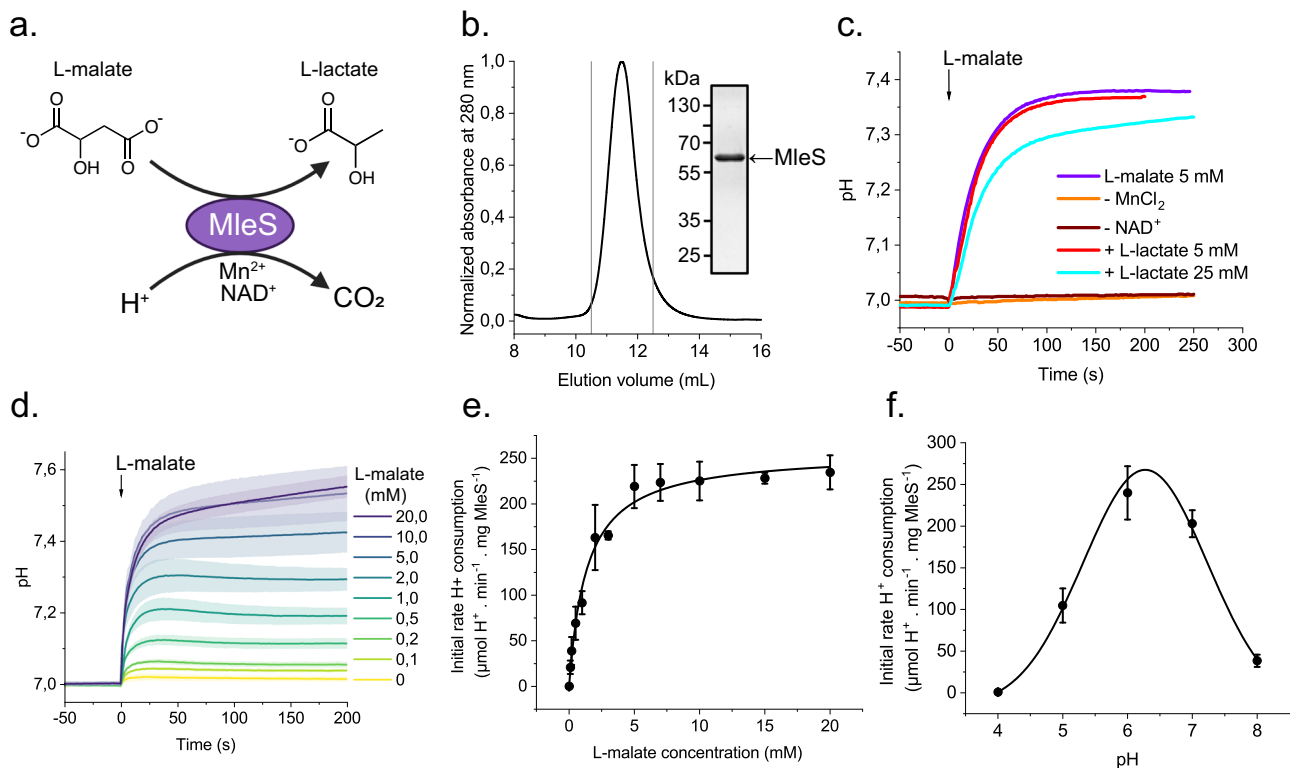


**Fig. 2 | L-malate decarboxylation activity of MleS.** **a** L-malate decarboxylation reaction catalyzed by MleS. **b** Representative size-exclusion chromatogram of MleS and SDS-polyacrylamide gel showing purified MleS. Similar results were obtained from three independent purification trials. (Uncropped gel in Supplementary Fig. 27). **c** pH traces were recorded with a pH microelectrode for the L-malate decarboxylation reaction at 30 °C and pH 7. The reaction started with the addition of 5 mM Na-L-malate at  $t = 0$ . pH traces in the absence of Mn<sup>2+</sup> and NAD<sup>+</sup> and in the presence of 5 mM and 25 mM of Na-L-lactate are indicated. pH was recorded at intervals of 1 s. **d** pH curves obtained for the decarboxylation reaction at different concentrations of Na-L-malate using 150 nM MleS and pH 7. pH curves correspond to the mean from independent experiments with different enzyme preparations ( $n = 3$ ). Shaded regions correspond to  $\pm$  SD. **e** L-malate dependence of MleS calculated from the initial rates of alkalization (first 10 seconds) obtained from pH curves in **d**, and using a titration curve (Supplementary Fig. 5) to convert pH

changes into  $\mu\text{mol of H}^+$ . Solid line corresponds to a Michaelis-Menten fit of the experimental data ( $R^2 = 0.987$ ). **f** pH dependence of the initial rates of H<sup>+</sup> consumption obtained for the decarboxylation of 5 mM Na-L-malate in low buffered solution at 30 °C and using 150 nM of enzyme. For pHs 4–5 the buffer solution was 2 mM of K-acetate, while for pHs 6–8 the buffer consisted of 2 mM K-phosphate. Initial rates of H<sup>+</sup> consumption were calculated as indicated in **e**, using distinct titration curves for every pH. The solid line corresponds to the fitting of experimental data to a logistic peak function ( $R^2 = 0.992$ ). Data points in **e** represent the mean of the H<sup>+</sup> consumption rate  $\pm$  SD ( $n = 3$ ) from independent experiments with different enzyme preparations. Data points in **f** represent the mean of the H<sup>+</sup> consumption rate  $\pm$  SD ( $n = 3$ ) from independent experiments with the same enzyme preparation. **a** was created with Biorender.com released under a Creative Commons Attribution-NonCommercial-NoDerivs 4.0 International license.

production of a monodisperse protein (Fig. 2b). The L-malate decarboxylation activity of MleS was determined by pH measurements in 2 mM of potassium phosphate and is presented as  $H^+$  consumption rate ( $\mu\text{mol } H^+ \text{ consumed min}^{-1} \text{ mg MleS}^{-1}$ ) (Fig. 2c–f). The  $H^+$  consumption was calibrated by titration of the reaction buffer with NaOH (Supplementary Fig. 5). We noticed that on longer timescales the amount of consumed  $H^+$  was lower than expected for a reaction with a  $K_{\text{eq}}$  of  $5.5 \times 10^2$ , calculated by eEquilibrator<sup>33</sup> (Supplementary Fig. 6d). To verify if the enzymatic reaction was not running to completeness, we followed the production of L-lactate by HPLC after derivatization with 9-chloromethyl anthracene (Supplementary Fig. 6). Virtually complete decarboxylation of 5 mM L-malate was confirmed by the production of approximately 5 mM of L-lactate (Supplementary Fig. 6d). We explain the leveling off of the pH by the dissolution of  $\text{CO}_2$  and the formation of bicarbonate plus a proton, which opposes the alkalization of the decarboxylation reaction. The pH recordings and L-lactate measurements show excellent correspondence for the initial 30 s of the reaction (Supplementary Fig. 6d, inset), and therefore, the initial rates of  $H^+$  consumption

were used to determine the kinetic parameters of MleS (Table 1 and Fig. 2c–f). There is no deleterious effect of L-lactate up to 5 mM (Fig. 2c and Supplementary Fig. 7), but the initial rate of  $H^+$  consumption was reduced by 50% in 25 mM L-lactate (Fig. 2c). The  $K_{\text{m}}^{\text{app}}$  for L-malate is  $1.4 \pm 0.4 \text{ mM}$  and  $K_{\text{m}}^{\text{app}}$  for  $\text{NAD}^+$  is  $42 \mu\text{M}$  (Supplementary Fig. 8) at pH 7. In summary, we show that MleS is a relatively fast enzyme with a  $k_{\text{cat}}$  of  $266 \pm 14 \text{ s}^{-1}$  around pH 7.

### L-malate decarboxylation pathway generates PMF in vesicles

**Quantification of the  $H^+$  gradient ( $\Delta\text{pH}$ ).** We determined the coupled activities of MleP and MleS in vesicles in which we first reconstituted MleP and then encapsulated MleS, along with  $\text{NAD}^+$  plus  $\text{MnCl}_2$  (Fig. 3a). We used MleS concentrations and MleP LPRs that would yield at least one dimer, even in the smallest vesicles ( $\sim 100 \text{ nm}$ ); the other components were encapsulated in a large excess (Table 2). We encapsulated the hydrophilic fluorescent probe pyranine (8-hydroxypyrene-1,3,6-trisulfonic acid or HPTS) for ratiometric quantification of the intravesicular pH (Supplementary Fig. 10). Preliminary experiments with liposomes showed that a small

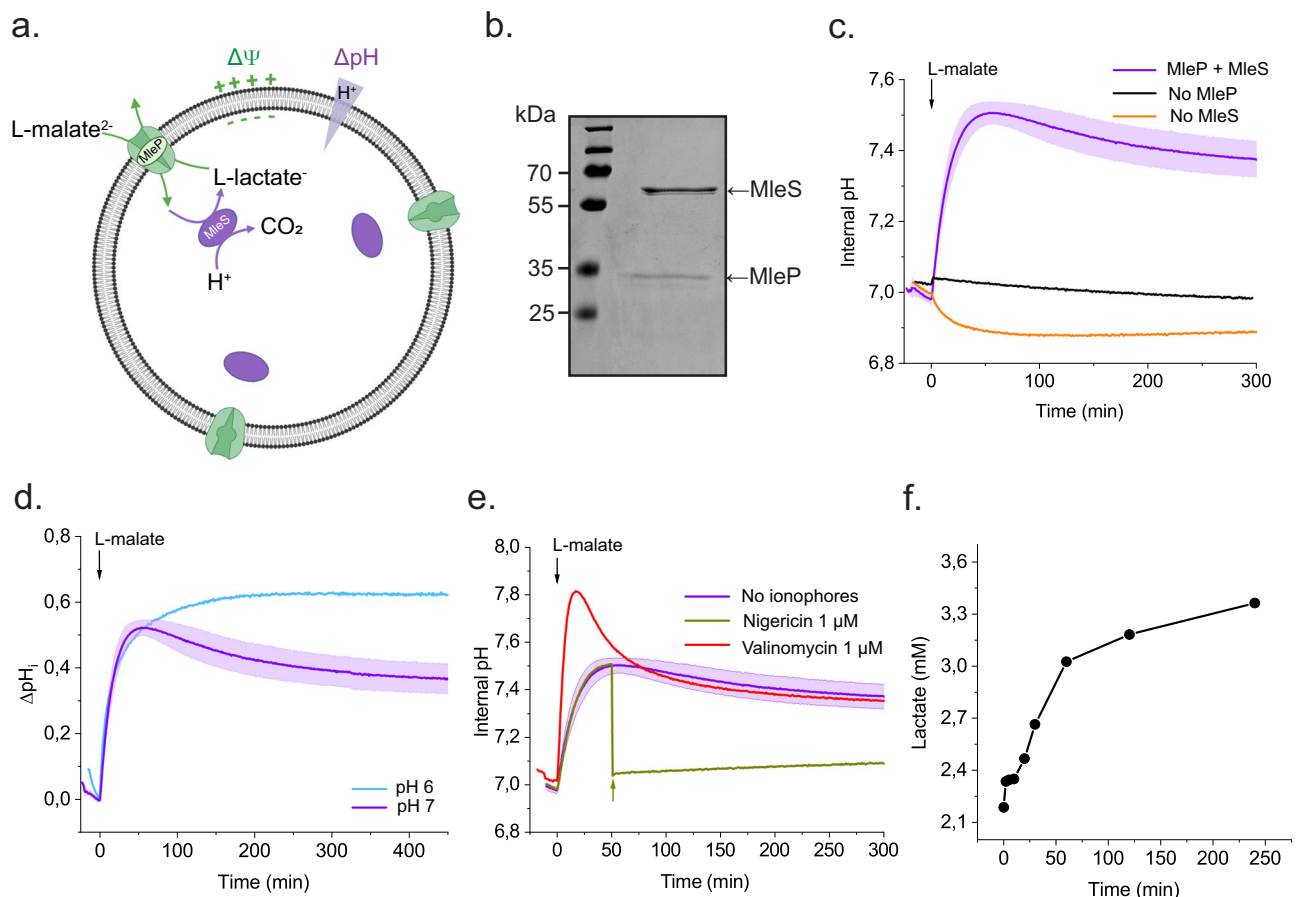


### Fig. 3 | Internal alkalization by the L-malate decarboxylation pathway.

**a** Cartoon of the L-malate decarboxylation pathway in liposomes. The consumption of  $H^+$  leads to an internal alkalization and thus a  $\Delta\text{pH}$  (alkaline inside) across the membrane (violet). The electrogenic exchange of internal L-lactate by external L-malate mediated by MleP generates a  $\Delta\Psi$  (negative inside) (green). **b** SDS-polyacrylamide gel of MleP LPR 250 (w/w) proteoliposomes in *E. coli* polar lipid:egg PC 3:1 (mol ratio) with  $2.5 \mu\text{M}$  MleS encapsulated. (Uncropped gel in Supplementary Fig. 9). **c** Internal pH of full system (MleP+MleS) reported by pyranine ( $n = 5$ ) or only MleS (No MleP,  $n = 2$ ) or only MleP (No MleS,  $n = 2$ ). Na-L-malate was added at  $t = 0$  to start the decarboxylation pathway (downward arrow). **d** Effect of pH on the  $\Delta\text{pH}$  formed by the L-malate decarboxylation pathway reconstituted in liposomes. **e** Effect of dissipation of  $\Delta\Psi$  (red,  $n = 3$ ) and  $\Delta\text{pH}$  (dark yellow) on the

internal pH (as indicated in **c**) with valinomycin or nigericin, respectively. Valinomycin was present before addition of L-malate and nigericin addition is indicated by an upward arrow. **f** Total L-lactate produced from the L-malate decarboxylation pathway (as in **c**), quantified by RP-HPLC after 9-CMA derivatization. Data points correspond to the mean of L-lactate concentration from independent replicates with different sample preparations ( $n = 2$ ). Internal pH curves in **c–e** correspond to the mean of pH from  $n$  independent experiments with different preparations of proteoliposomes. pH curves were calculated from the ratio of the pyranine fluorescence intensities at the excitation wavelengths 450 nm and 405 nm, using the calibration curve in Supplementary Fig. 10. Shaded areas represent  $\pm \text{SD}$ . **a** was created with Biorender.com released under a Creative Commons Attribution-NonCommercial-NoDeriv 4.0 International license.

**Table 2 | Approximate number of components of the L-malate decarboxylation pathway (MleP and MleS), co-reconstituted solute transporters (GltP and LacY) and enzymes of the lactose metabolism pathway ( $\beta$ -galactosidase (LacZ), hexokinase (HK) and glucose-6-phosphate dehydrogenase (G6P-DH)) in vesicles composed of *E. coli* polar lipids:egg PC 3:1 (mol ratio)**

Component	Molecular weight	Oligomeric unit	Internal concentration	Molecules per vesicle		
				100 nm	200 nm	400 nm
MleP	47.9 kDa	Dimer <sup>i</sup>	LPR 250 (w/w)	6 (3)	25 (12)	100 (50)
MleS	62.1 kDa	Dimer <sup>ii</sup>	2.5 $\mu$ M	2	8	48
NAD <sup>+</sup>			1 mM	246	2230	19000
Mn <sup>2+</sup>			0.5 mM	125	1125	9500
L-lactate <sup>-</sup>			2 mM	500	4500	38000
Pyranine			0.1 mM	25	223	1900
GltP	48.8 kDa <sup>iii</sup>	Trimer <sup>iv</sup>	LPR 250 (w/w)	6	25	100
LacY	46.5 kDa	Monomer <sup>v</sup>	LPR 200 (w/w)	6	25	100
LacZ	116.3 kDa	Tetramer <sup>vi</sup>	7 $\mu$ M	2	16	130
HK	53.7 kDa	Monomer-Dimer <sup>vii</sup>	7 $\mu$ M	2	16	130
G6P-DH	57.4 kDa	Dimer-Tetramer <sup>viii</sup>	4 $\mu$ M	1	10	80

Molecular weight indicated for subunits. The number of molecules per vesicle is calculated from the internal concentration and volume of the vesicle or lipid-to-protein ratios (for the membrane proteins); we assume a homogeneous distribution of the components over the large-unilamellar vesicles; the enzyme concentrations/numbers reflect those of the subunits and not the structural complexes. The number of molecules of MleP in parenthesis is based on the 50% reconstitution efficiency. <sup>i</sup>As determined for homologs of 2HCT family<sup>26</sup>. <sup>ii</sup>Determined for homologs<sup>30,31</sup>. <sup>iii</sup>Taken from ref. 24. <sup>iv</sup>Taken from ref. 93. <sup>v</sup>Taken from ref. 25. <sup>vi</sup>Taken from ref. 94. <sup>vii</sup>Taken from ref. 95. <sup>viii</sup>Taken from ref. 96.

fraction of pyranine is retained at the outer surface of the vesicles, even after extensive washing (two cycles of ultracentrifugation and resuspension, and a final gel filtration step) (Supplementary Fig. 11). Therefore, we included the collisional quencher DPX (p-xylene-bispyridinium bromide) in the external medium for every measurement<sup>34</sup>. Additionally, we inhibited any MleS, possibly adsorbed to the outer surface of the vesicles, by using EDTA to chelate Mn<sup>2+</sup> ions that are required for activity (Supplementary Fig. 12a). Due to the low rate of L-malate uniport by MleP (Fig. 1f), we included 2 mM of L-lactate inside the vesicles to enable rapid L-malate/L-lactate exchange. We kept the same concentration in the external medium, because L-lactic acid (in fast equilibrium with L-lactate) rapidly permeates the membrane (Supplementary Fig. 18a). Indeed, when L-lactate is not initially present in the external medium, the alkalization is slower because initially, only L-malate uniport is possible, but the internal pH reaches a higher point than in the presence of external L-lactate (Supplementary Fig. 13).

Upon addition of 10 mM L-malate to the MleP-MleS containing vesicles, the internal pH increased from 7.0 to 7.50  $\pm$  0.03 (Fig. 3c) and then over a period of 10 h gradually decreased to 7.34  $\pm$  0.07 (Supplementary Fig. 14). The drop in internal pH was not observed at pH 6.0 (Fig. 3d). No alkalization was observed when either MleP or MleS were absent (Fig. 3c), indicating that the formation of a pH gradient ( $\Delta$ pH) requires the coupled activities of MleP and MleS. The rate of alkalization increases with lower LPR (more MleP per vesicle) and higher amounts of encapsulated MleS (Supplementary Fig. 15). Although the  $k_{cat}$  of the enzymatic reaction is  $\approx$ 10 $\times$  higher than the estimated turnover number of MleP, the MleP/MleS ratio (in molecules per vesicle) was always higher than 1 (range 2–13), explaining the increase in activity with MleS concentration (Supplementary Fig. 15). However, the rate of acidification shows a stronger dependence on the MleP than MleS concentration. A slight decrease in internal pH was observed upon addition of L-malate to vesicles lacking MleS (Fig. 3c), which may reflect uniport of L-malateH<sup>-</sup> and dissociation of the proton in the vesicle lumen.

To demonstrate that the internal alkalization results in a H<sup>+</sup> gradient across the membrane we used the ionophore nigericin, which exchanges K<sup>+</sup> for H<sup>+</sup>. Indeed, nigericin collapses the H<sup>+</sup> gradient (Fig. 3e). The formation of a membrane potential by L-malate decarboxylation is evident from the accelerated alkalization in the presence of the K<sup>+</sup>-selective ionophore valinomycin, which dissipates the membrane potential  $\Delta\Psi$  (Fig. 3e). The  $\Delta\Psi$

(inside negative) slows down the L-malate/L-lactate exchange decreasing thereby the activity of the L-malate decarboxylation pathway.

Interestingly, when the L-malate decarboxylation pathway runs at pH 6, which is the optimal pH for MleS and MleP (Figs. 1e and 2f), the H<sup>+</sup> gradient is maintained constant for longer periods of time (Fig. 3d). Finally, CO<sub>2</sub> can leave the vesicles by passive diffusion but it can also be converted into bicarbonate plus a proton and thus contribute to acidification of the vesicle lumen.

**Quantification of membrane potential ( $\Delta\Psi$ ).** Next, we monitored the formation of the  $\Delta\Psi$ , using the fluorescent probe DiSC<sub>3</sub>(5) (3,3'-dipropylthiadicarbocyanine iodide)<sup>35,36</sup>. This carbocyanine distributes uniformly over the inner and outer leaflet when  $\Delta\Psi = 0$  (Fig. 4a).  $\Delta\Psi < 0$  leads to accumulation of the probe in the inner leaflet and quenching of fluorescence (Fig. 4a, b). After equilibration of DiSC<sub>3</sub>(5) in the membrane of L-lactate-loaded MleP vesicles, the addition of 10 mM L-malate results in a fast quenching of fluorescence (Fig. 4b). This indicates the generation of  $\Delta\Psi < 0$  as a consequence of the L-malate/L-lactate exchange. The exchange rapidly reaches electrochemical equilibrium, in which the L-malate gradient is opposed by the  $\Delta\Psi$ , after which the membrane potential slowly decreasing (Fig. 4b). When the same experiment is performed with MleP vesicles containing MleS, a larger quenching is observed (Fig. 4b). The internal conversion of L-malate into L-lactate, catalyzed by MleS, maintains the inward gradient of L-malate and hence, the membrane potential is larger and sustained for a longer period of time (Fig. 4b). Competition between L-malate and L-lactate leads to a gradual decrease in  $\Delta\Psi$ , because fewer molecules of L-malate are transported per unit of time when the L-lactate concentration in the external medium increases. The dissipation of  $\Delta\Psi$  starts earlier than the dissipation of  $\Delta$ pH, which reflects the low capacitance of the lipid bilayer as the translocation of a few charges is sufficient to reduce  $\Delta\Psi$  substantially.

The dequenching of DiSC<sub>3</sub>(5) fluorescence upon addition of valinomycin confirms that the L-malate-induced quenching corresponds to the formation of a  $\Delta\Psi$  across the membrane. We calibrated the fluorescence quenching by comparison of the signal generated with K<sup>+</sup> diffusion potentials of varying magnitudes (Supplementary Fig. 16). We find  $\Delta\Psi = -79 \pm 9$  mV three min after addition of L-malate when the decarboxylation reaction is done at pH 7 (Fig. 4b, d). Similar as seen with the  $\Delta$ pH, the build-up of  $\Delta\Psi$  is faster and subsequent dissipation

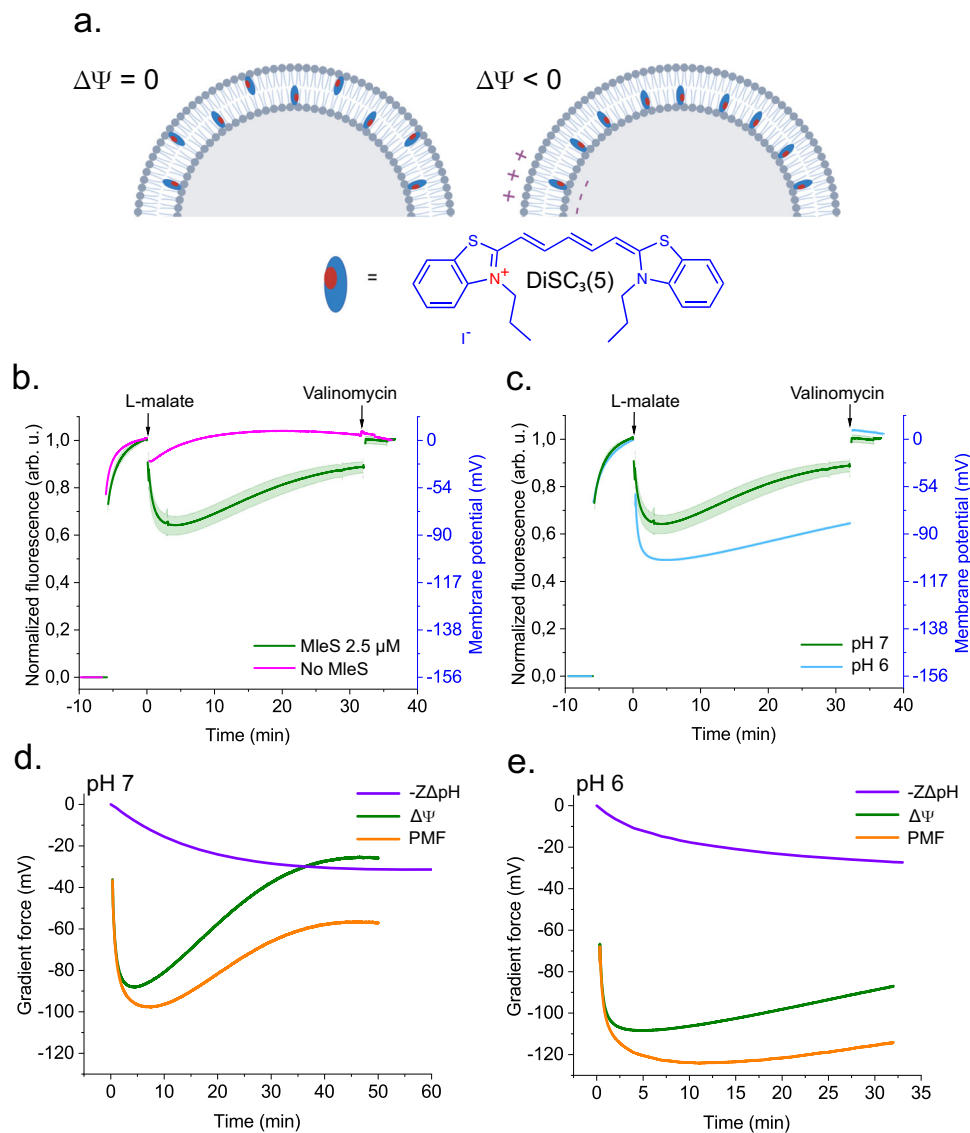


**Fig. 4 | Dynamics of the membrane potential and PMF.** **a** The fluorescent probe 3,3'-dipropylthiadicarbocyanine iodide (DiSC<sub>3</sub>(5)) distributes in response to a membrane potential ( $\Delta\Psi$ ). **b** DiSC<sub>3</sub>(5) fluorescence curves generated for MleP LPR 250 proteoliposomes containing MleS ( $n = 3$ ) or no MleS ( $n = 2$ ). After equilibration of DiSC<sub>3</sub>(5), L-malate was added at  $t = 0$  and the fluorescence quenching effect was recorded. At the end valinomycin was added to dissipate the  $\Delta\Psi$ . **c** Effect of pH on the DiSC<sub>3</sub>(5) fluorescence curve for the L-malate decarboxylation pathway ( $n = 1$ ). Conditions of the measurements at pH 6 are the same as those at pH 7, but the internal and external buffer was K phosphate pH 6. Measurements were performed at 30 °C. Solid lines correspond to the fluorescence data normalized to the point immediately before L-malate addition and are presented in arbitrary units (arb. u.). Data in green curves represent the mean of fluorescence from independent experiments with  $n$  different preparations of proteoliposomes. Shaded areas in **(b, c)**, indicate  $\pm$  SD. Membrane potential was calculated from calibration data

(Supplementary Fig. 16) and is presented in the right axis. **d** Gradient forces calculated from the pH gradient and membrane potential data at pH 7. **e** Gradient forces calculated from the  $\Delta$ pH and membrane potential data at pH 6. pH curves after addition of 10 mM L-malate (violet) were taken from Fig. 3d and the driving forces were calculated from  $Z\Delta p\text{H} = 2.303(RT/F)\Delta\text{pH}$ , where  $R$  is the gas constant ( $8.31\text{ J mol}^{-1}\text{ K}^{-1}$ ),  $T$  is temperature in Kelvin (303 K) and  $F$  is the Faraday constant ( $96485\text{ C mol}^{-1}$ ).  $\Delta\text{pH}$  was determined assuming that at  $t = 0$   $\text{pH}_i = \text{pH}_o$ , and that the external pH does not change substantially. Since  $\Delta\text{pH}$  is a positive value ( $\text{pH}_i - \text{pH}_o$ ), the plotted curve corresponds to  $-\Delta\text{pH}$ . Membrane potential ( $\Delta\Psi$ ) data (green) were calculated by interpolation of the fluorescence quenching from panel c and Supplementary Fig. 18b, using the calibration curve from Supplementary Fig. 16b. Proton motive force (PMF) curves were calculated from  $-\Delta\text{pH}$  plus  $\Delta\Psi$ . **a** was created with Biorender.com released under a Creative Commons Attribution-NonCommercial-NoDerivs 4.0 International license.

occurs at a lower rate when the pathway is operated at pH 6 (Fig. 4c, e), which is in line with the activity of MleP and MleS.

The dynamics of the PMF generated by the L-malate decarboxylation at pH 7 and 6 follows from the corresponding  $\Delta\text{pH}$  and  $\Delta\Psi$  curves, using Eq. 1 (Fig. 4d, e, orange curves). The PMF shows similar dynamics as the membrane potential and is maintained at a higher level at pH 6 than pH 7. In line with the low electrical capacitance of lipid bilayers and the relatively high buffer capacity of the internal medium the  $\Delta\Psi$  is formed faster than the  $\Delta\text{pH}$  and is initially the main component of the PMF at pH 7.

### PMF from L-malate decarboxylation fuels the transport of glutamate

Next, we used the  $\Delta\Psi$  and  $\Delta\text{pH}$  formed by L-malate decarboxylation to drive the accumulation of L-glutamate and D-lactose. We over-expressed and purified GltP of *E. coli* and co-reconstituted the protein with MleP in vesicles composed of *E. coli* polar lipids:egg PC 3:1 (Fig. 5a). Both proteins were co-reconstituted at relatively high LPR (250 each) to assure a high reconstitution efficiency<sup>37,38</sup>. Cryo-TEM shows the size-distribution and the predominantly unilamellar nature of the vesicles (Supplementary Fig. 17a). Estimation of the

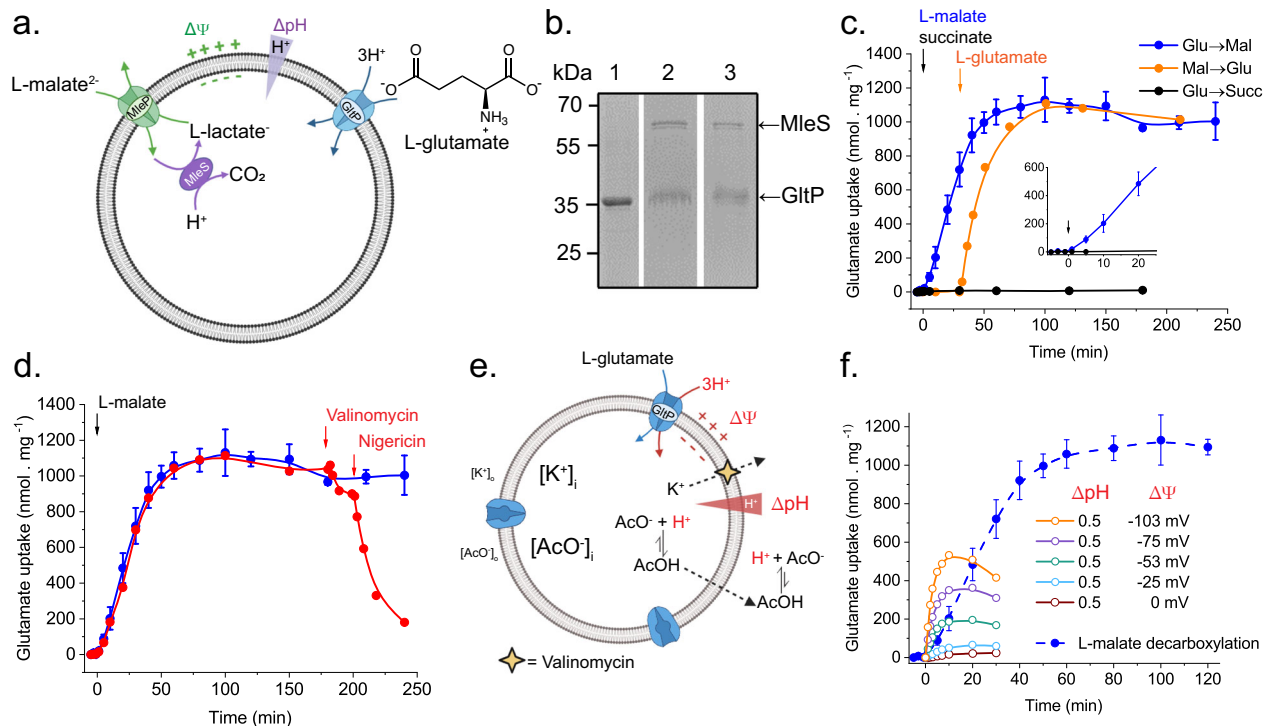


**Fig. 5 | L-glutamate transport driven by the PMF from the L-malate decarboxylation pathway.** **a** Cartoon of the co-reconstituted L-malate decarboxylation pathway and GltP in liposomes. The coupled transport of  $3\text{H}^+$  and 1 L-glutamate by GltP is driven by the PMF from the L-malate decarboxylation pathway. **b** SDS-polyacrylamide gel of purified GltP in DDM (Lane 1), reconstituted at LPR 100 (w/w) (Lane 2), and co-reconstituted with MleP at LPR 100 (w/w) (Lane 3) in *E. coli* polar lipids:egg PC 3:1 (mol ratio) liposomes. MleS was encapsulated in the vesicles of Lane 2 and 3. (Uncropped gel in Supplementary Fig. 1b). **c** Glutamate transport upon addition of 10 mM L-malate in MleP LPR 250 - GltP LPR 250 proteoliposomes containing L-malate decarboxylation components. In curves blue and black, proteoliposomes were pre-incubated for 5 min with external  $20\ \mu\text{M}$  Na- $^{14}\text{C}$ -glutamate before addition of 10 mM of L-malate (blue) or succinate (black) (Glu→Mal and Glu→Succ). In the orange curve, 10 mM L-malate was added at  $t = 0$ , and, after 30 min of incubation, the uptake was started by addition of  $20\ \mu\text{M}$  Na-

$^{14}\text{C}$ -glutamate (Mal→Glu). **d** Dissipation of  $\Delta\Psi$  and  $\Delta\text{pH}$  by  $1\ \mu\text{M}$  valinomycin and  $1\ \mu\text{M}$  nigericin, respectively, at  $t = 3$  h. Data correspond to an individual experiment with a single preparation of proteoliposomes. **e** Cartoon of the L-glutamate transport (in symport with  $\text{H}^+$ ) driven by  $\Delta\Psi$  and  $\Delta\text{pH}$ , which are formed by valinomycin-mediated  $\text{K}^+$  diffusion ( $\Delta\Psi$ ) and acetate ( $\text{AcO}^-$ )/acetic acid ( $\text{AcOH}$ ) diffusion ( $\Delta\text{pH}$ ) potentials in GltP liposomes. **f** Comparison of the L-glutamate transport driven by the PMF from the L-malate decarboxylation pathway (blue) with that from  $\text{K}^+$  and acetate diffusion potentials in MleP-GltP proteoliposomes ( $n = 1$ ). All the experiments were performed at  $30\ ^\circ\text{C}$  and pH 7. Data for the blue curves in (c, d, and f) are presented as the mean of L-glutamate uptake (nmol of internalized L-glutamate per mg of GltP)  $\pm$  SD from independent replicates ( $n = 5$ ) with different preparations of proteoliposomes. **a, e** were created with Biorender.com released under a Creative Commons Attribution-NonCommercial-NoDerivs 4.0 International license.

incorporation efficiency of GltP and MleP in the same vesicles was not possible by SDS-PAGE, because both proteins migrate similarly. Individually, they were reconstituted with an efficiency of 60 and 50%, respectively (Fig. 5b & Supplementary Fig. 1a, b). MleS,  $\text{NAD}^+$ ,  $\text{Mn}^{2+}$ , sodium-L-lactate plus pyranine were encapsulated in the MleP-GltP vesicles. Co-incorporation of GltP did not significantly affect the performance of the L-malate decarboxylation pathway (Supplementary Fig. 19a). Addition of L-glutamate leads to a small drop in the pH gradient, which is in agreement with  $3\text{H}^+$  symported with L-glutamate by GltP (Supplementary Fig. 19b).

Figure 5c shows the uptake of L-glutamate, driven by the PMF that is generated by L-malate decarboxylation. After 40–50 min a steady state is reached, which lasts at least 4 hours; the accumulation level ( $[\text{Glu}]_{\text{IN}}/[\text{Glu}]_{\text{OUT}}$ ) is  $\sim 140$  (based on a specific internal volume of  $3\ \mu\text{L}/\text{mg}$  of lipid<sup>39</sup>) (Fig. 5c & Supplementary Fig. 20). The uptake of L-glutamate is sigmoidal, because it takes some time to generate the PMF. When the transport reaction is initiated 30 min after the start of the L-malate decarboxylation (i.e., pre-formed PMF), there is no delay and the initial glutamate uptake increases linearly with time (compare blue and orange lines, Fig. 5c). There is no transport of L-glutamate when succinate instead of L-malate is used (Fig. 5c, inset). The rate of L-glutamate uptake depends on the L-glutamate concentration with a  $K_m^{\text{app}} = 33\ \mu\text{M}$  (Supplementary Fig. 20). In line with the effect on the PMF (Figs. 3d and 4c), the rate of glutamate transport driven by the

L-malate decarboxylation at pH 6 is not substantially different from that at pH 7 but the accumulation level is higher at pH 6 (Supplementary Fig. 21), which is in agreement with the higher driving force. The accumulation level of  $\sim 140$  matches the  $\Delta\text{pH}$  (0.5 pH units) and  $\Delta\Psi$  ( $\sim 20$  mV) at pH 7 obtained 50 min after L-malate addition (Fig. 4d) and the  $\text{H}^+$ /glutamate- stoichiometry of 3. Equation 2 yields a  $[\text{Glu}]_{\text{IN}}/[\text{Glu}]_{\text{OUT}}$  of  $\sim 150$ -fold for the PMF generated by L-malate decarboxylation, indicating a good correspondence between the generated driving force and the formed glutamate gradient via GltP.

$$2\Delta\Psi - 3\frac{RT}{F} \cdot 2.3\Delta\text{pH} = \frac{RT}{F} \cdot 2.3\log\left(\frac{[\text{Glu}^-]_{\text{IN}}}{[\text{Glu}^-]_{\text{OUT}}}\right) \quad (2)$$

Accumulated L-glutamate leaves the vesicles when  $\Delta\Psi$  and  $\Delta\text{pH}$  are dissipated by the action of the ionophores valinomycin and nigericin (Fig. 5d). Addition of valinomycin (a highly selective  $\text{K}^+$  ionophore) leads to a transient pH increment and dissipation of the membrane potential, which results in a small efflux of glutamate. The total PMF is dissipated upon subsequent addition of nigericin (an ionophore that exchanges  $\text{K}^+$  for  $\text{H}^+$ ), and efflux of glutamate to equilibrium levels is observed. Since the  $\Delta\text{pH}$  acts three times as driving force, whereas the  $\Delta\Psi$  acts twice (See Eq. 2), the dissipation of  $\Delta\Psi$  has less effect on the steady state levels of glutamate than  $\Delta\text{pH}$  dissipation. In line with this, lower but sustained levels of glutamate are observed

when valinomycin was present from the beginning of the experiment (Supplementary Fig. 22b).

The power of the L-malate decarboxylation pathway is not only demonstrated by the high levels of L-glutamate uptake, but also by the maintenance of large solute gradients for hours. This is especially clear when L-glutamate accumulation driven by the L-malate decarboxylation is compared with the transport driven by a  $K^+$  diffusion potential together with an acetic acid diffusion potential, which is the generic approach to study PMF-dependent transport processes<sup>40,41</sup> (Fig. 5e). Dilution of MleP-GltP vesicles, containing Na-acetate, into a solution with a lower concentration of Na-acetate establishes an inward  $H^+$  gradient as a consequence of the outward passive diffusion of acetic acid (Fig. 5e). The  $\Delta pH$  is proportional to the in/out ratio of the acetate concentration (See Methods). Along with a negative-inside  $\Delta\Psi$ , generated by valinomycin-mediated outward  $K^+$  diffusion, the two gradients yield a transient PMF (Fig. 5e) that we used as benchmark for the PMF from the L-malate decarboxylation pathway. With an artificially-imposed pH gradient of 0.5 (alkaline inside) and  $\Delta\Psi$  varying from 0 to  $-100$  mV, we determined the dependence of L-glutamate transport on the driving force (Supplementary Fig. 23b, c). The maximal rate is higher than with L-malate decarboxylation but L-glutamate leaks out after 10 min, because the  $\Delta\Psi$  and  $\Delta pH$  are transient (Fig. 5f and Supplementary Fig. 23b). Moreover, the acetate gradient yields a  $\Delta pH \approx 0.4$  that decreases slowly in the absence and rapidly in the presence of  $\Delta\Psi$  (inside negative) (Supplementary Fig. 23d). Thus, the transient nature of diffusion potentials and the interdependence of  $\Delta\Psi$  on  $\Delta pH$  and vice versa prohibit thermodynamic analyzes of transport reactions as exemplified here by Eq. 2. By contrast, the L-malate decarboxylation pathway yields smaller gradients but they can be kept constant for hours (Figs. 3 and 4).

By comparing the initial rate of L-glutamate uptake driven by the L-malate decarboxylation with the initial rates of glutamate uptake driven by diffusion potentials (Supplementary Fig. 23b–c), we estimate that the driving force from the L-malate decarboxylation is comparable to a  $\Delta pH$  of 0.5 (by acetate diffusion) and a membrane potential of  $-40$  mV (by valinomycin-mediated potassium diffusion) and thus a PMF of  $-70$  mV, which is in line with direct measurements of  $\Delta pH$  and  $\Delta\Psi$  by the fluorometric probes pyranine and DiSC<sub>3</sub>(5) (Fig. 4d).

### PMF from L-malate decarboxylation fuels the transport of lactose

We also co-reconstituted the L-malate decarboxylation pathway with *E. coli* lactose permease, LacY<sup>25</sup>, which functions as a  $H^+$ /galactoside symporter (Fig. 6a). The (co-)reconstitution protocol for LacY-MleP<sup>42–44</sup> differs from the one we used for GltP-MleP, but we obtained mostly unilamellar vesicles as shown by cryo-TEM (Supplementary Fig. 17b). We find that co-reconstitution mediated by octyl- $\beta$ -D-galactopyranoside (OG), and detergent removal via rapid dilution, generated the largest L-malate dependent D-lactose uptake (Supplementary Fig. 24). The  $\Delta pH$  formed by L-malate decarboxylation was comparable with and without LacY in the vesicles (see Supplementary Fig. 25 and Fig. 3d). D-lactose uptake reached its maximal level after 2 hours (Fig. 6c);  $[\text{lactose}]_{\text{IN}}/[\text{lactose}]_{\text{OUT}} \approx 20$  (or 75 mV). A slight reduction in accumulation level was observed at later times, presumably due to a decrease in PMF or as a result of an uncoupled lactose efflux. Since lactose is taken up with 1 proton the accumulation is much lower than for glutamate, which is symported with 3 protons; the  $[\text{lactose}]_{\text{IN}}/[\text{lactose}]_{\text{OUT}}$  gradient of 75 mV is in line with a PMF of  $-70$  mV (see Eq. 3).

$$\Delta\Psi - \frac{RT}{F} 2.3\Delta pH = \frac{RT}{F} 2.3\log\left(\frac{[\text{Lactose}]_{\text{IN}}}{[\text{Lactose}]_{\text{OUT}}}\right) \quad (3)$$

Thus, the L-malate decarboxylation pathway forms a PMF that is stable on the timescale of hours and allows the accumulation of lactose

and L-glutamate to a point of good correspondence between the generated PMF and the established solute gradient from the active transport.

### Coupling of L-malate-dependent lactose transport to carbohydrate metabolism

Next, we encapsulated  $\beta$ -galactosidase (LacZ), hexokinase (HK) plus glucose-6-phosphate dehydrogenase (G6P-DH) in MleP-LacY vesicles with L-malate decarboxylation pathway. These enzymes catalyze the hydrolysis of D-lactose into galactose and glucose, phosphorylation of glucose to glucose-6-phosphate (G6P, entry point for glycolytic pathway) and formation of 6-phosphoglucono- $\delta$ -lactone (pentose phosphate pathway) plus NADPH (Fig. 6d). The reduction of  $NADP^+$  to NADPH was used to monitor the activity of the overall pathway (Fig. 6e). We ran the L-malate decarboxylation for 30 min to pre-form a PMF and then added D-lactose, which elicits an increase in NADPH fluorescence that is not observed in vesicles without LacY (Fig. 6e). The NADPH fluorescence is reduced in the presence non-hydrolysable substrates methyl- $\beta$ -D-thiogalactoside (TMG) and thiodigalactoside (TDG) (Fig. 6e, f), which act as low ( $K_D \approx 1$  mM) and high ( $K_D = 30$ – $50$   $\mu$ M) affinity competitive inhibitors of lactose transport, respectively<sup>45–47</sup>. NADPH production is dependent on the D-lactose concentration with a half saturation constant ( $K_m^{\text{app}}$ ) of  $\approx 0.2$  mM, which is close to the apparent  $K_m$  for LacY (Fig. 6g, h and Table 1). In our design of the reaction network, the maximal levels of NADPH formed are determined by the amount  $NADP^+$  encapsulated in the vesicles; additional control experiments are shown in Supplementary Fig. 26a. Finally, NADPH was also formed in the absence of L-malate decarboxylation albeit at a lower rate. Since lactose is internally hydrolyzed, an out-to-in lactose gradient is maintained to facilitate the uptake of lactose. Furthermore, the galactose formed upon hydrolysis of lactose by LacZ is a substrate of LacY and enables lactose/galactose exchange, which is even faster than lactose- $H^+$  symport driven by the PMF (Supplementary Fig. 26b)<sup>45,48</sup>. Yet, the fastest metabolism of lactose is observed when a PMF is formed by the L-malate decarboxylation pathway and used to drive the uptake of lactose. We thus show full functionality of a reaction network involving (i) PMF generation by electrogenic transport and decarboxylation of L-malate; (ii) PMF consumption by lactose- $H^+$  symport; (iii) metabolism of lactose to galactose plus 6-phosphoglucono- $\delta$ -lactone; and (iv) reduction of  $NADP^+$  to NADPH.

### Discussion

We have developed a minimal PMF-generating system in lipid vesicles that enables the efficient uptake of nutrients via secondary active transporters. We show that transport of the amino acid L-glutamate and the sugar lactose, mediated by GltP and LacY, respectively, reach maximal accumulation levels in good agreement with the generated driving force. Furthermore, we have shown coupling of this chemiosmotic system to the initial steps of lactose metabolism and the formation of NADPH. This work is part of our efforts to construct synthetic cells from molecular components and the development of pathways for long-term fueling of energy requiring processes. In comparison to strategies to feed synthetic cells with building blocks by diffusion via pore-forming toxins<sup>49</sup>, nanopores<sup>50,51</sup> or low-selectivity channels<sup>52</sup>, the L-malate decarboxylation pathway and ion-linked transporters allow the accumulation of nutrients against their concentration gradient. This is an essential feature of living cells, not only to transport molecules in but also to pump metabolic end products out. Additionally, the components of the system presented here are proteins that can be expressed and regenerated from their genetic units by an encapsulated transcription-translation machinery, contributing to the construction of an autonomous synthetic cell<sup>53,54</sup>.

Besides the sustained chemiosmotic transport of nutrients, our study offers kinetic and mechanistic insights into the two protein components of the L-malate decarboxylation pathway (Figs. 1 and 2).

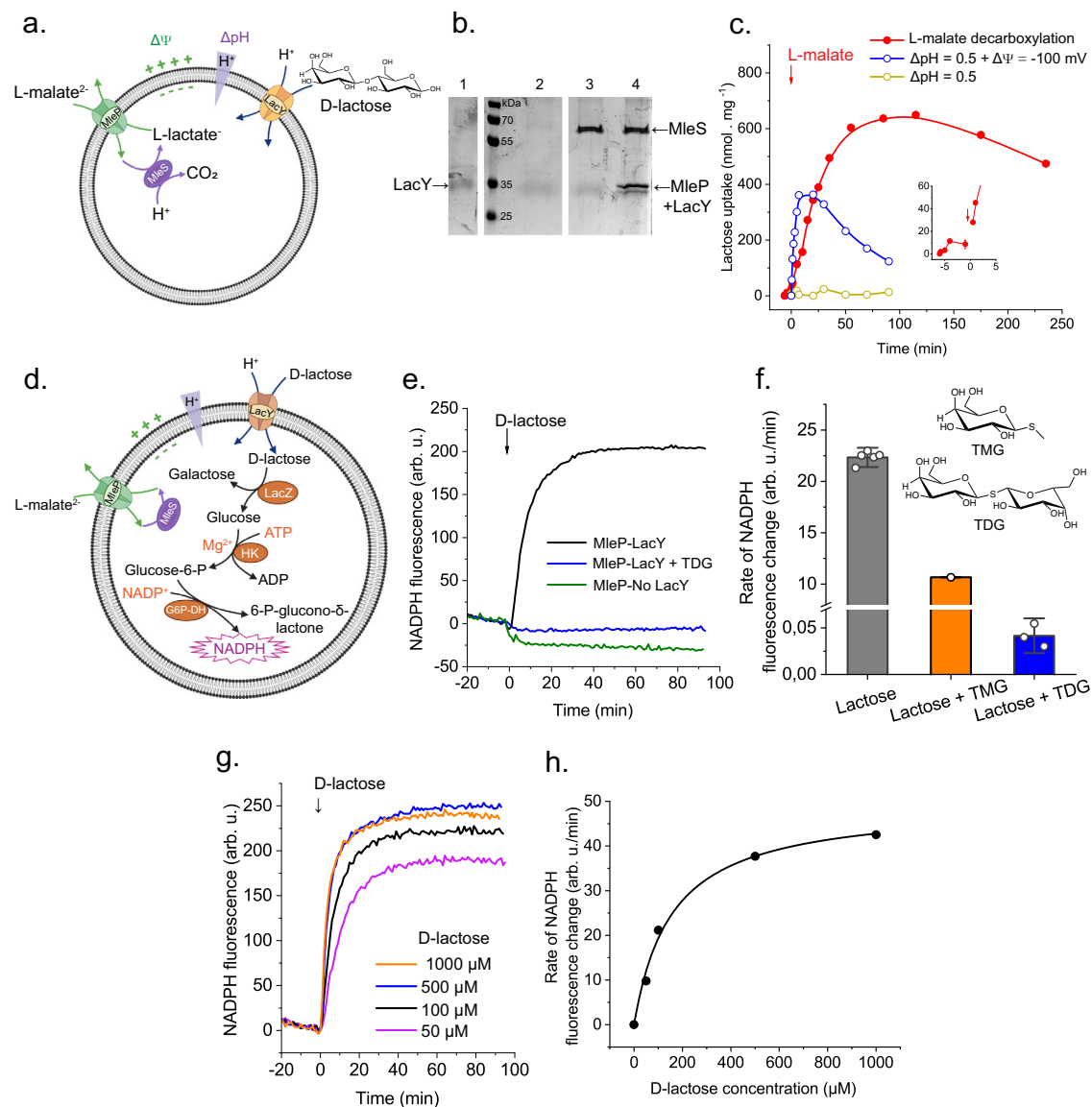


**Fig. 6 | D-lactose transport and coupling to internal carbohydrate metabolism.**

**a** Cartoon of the co-reconstituted L-malate decarboxylation pathway and LacY in liposomes. **b** SDS-polyacrylamide gel of purified LacY (Lane 1), reconstituted at LPR 100 (w/w) (Lanes 2 and 3). Lane 4, co-reconstituted MleP LPR 100 (w/w) and LacY LPR 100 (w/w). Samples of lanes 3 and 4 contained MleS. Lipid system: *E. coli* polar lipids: egg PC 3:1 (mol ratio). Uncropped gel in Supplementary Fig. 1c. **c** Comparison of the L-malate-induced  $^{14}\text{C}$ -D-lactose transport driven by the L-malate decarboxylation (red) with transport driven by a  $\Delta\text{pH}$  generated from acetate diffusion with (blue) and without (yellow) valinomycin-mediated  $\Delta\Psi$  in MleP LPR 250–LacY LPR 200 (w/w) proteoliposomes. Inset: zoom in on the initial D-lactose uptake curve. Data in the red curve represent the mean of D-lactose uptake (nmol of D-lactose  $\text{mg}^{-1}$  LacY) from  $n = 2$  independent replicates with different preparations of proteoliposomes. **d** Cartoon of vesicles with L-malate decarboxylation pathway plus reaction for hydrolysis of lactose (LacZ), phosphorylation of glucose by hexokinase (HK), using Mg-ATP, and oxidation of glucose-6-phosphate (G6P-DH),

using  $\text{NADP}^+$ . **e** NADPH production in vesicles with MleP-LacY (black and blue) or only MleP (green) plus MleS, LacZ, HK, and G6P-DH. L-malate decarboxylation was started by addition of 10 mM Na-L-malate 30 min before D-lactose (100  $\mu\text{M}$ ) addition at  $t = 0$  in absence (black and green) or presence (blue) of 20 mM of non-hydrolysable thiodigalactoside (TDG). Data correspond to the mean of fluorescence from 5 (black), 3 (blue) and 2 (green) technical replicates. **f** Effect of 20 mM methyl- $\beta$ -D-thiogalactoside (TMG) or TDG on the lactose metabolism. Error bars indicate  $\pm$  SD from 5 (gray) and 3 (blue) technical replicates. **g** D-lactose dependence of NADPH production in MleP-LacY vesicles. **h** D-lactose dependence of NADPH production presented as the initial rate of NADPH fluorescence change. Solid line represents a Michaelis-Menten fit to experimental data ( $R^2 = 0.991$ ). The half saturation constant = 0.2 mM. NADPH fluorescence was followed at excitation of 350 nm and emission of 460 nm (slit width of 5 nm). **a**, **d** were created with Biorender.com released under a Creative Commons Attribution-NonCommercial-NoDerivs 4.0 International license.

Particularly, the association of the half turnover electrical signals (Fig. 1g, h) with the presence of a highly conserved positively charged residue in the binding pocket of 2HCT family members<sup>55,56</sup> suggests that the preferred species transported by MleP are the mono-protonated forms of L-malate ( $\text{HMal}^-$ ) and L-lactate (L-lactic acid). Thus, we conclude that MleP generates a membrane potential by mono-anionic L-malate/L-lactic acid antiport or at a much lower rate by mono-anionic L-malate uniport.

The L-malate decarboxylation pathway is a particularly useful and robust system for the provision of metabolic energy in the form of a PMF, because: (i) The L-malate decarboxylation pathway is constituted of only two proteins: an integral membrane protein that works as an electrogenic MleP and a soluble enzyme that catalyzes the decarboxylation of L-malate to L-lactate (MleS). Decarboxylation pathways involving an electrogenic exchange or antiport reaction are arguably the simplest mechanisms to generate an

electrochemical proton gradient across the membrane. (ii) MleP exchanges structurally related substrates, L-malate and L-lactic acid, which have in common the 2-hydroxycarboxylate unit. The direction of transport is determined by the substrate concentration gradients and not by the orientation of MleP in the membrane<sup>57,58</sup>. Indeed, we show that an inside negative potential is formed when L-malate is taken up in exchange for internal L-lactate, whereas a positive potential is formed for L-malate exit in exchange for external L-lactate (Fig. 1). This is a technical advantage over primary transporters that facilitate H<sup>+</sup> translocation in a light-dependent process<sup>59,60</sup>, a redox reaction<sup>61</sup> or ATP hydrolysis<sup>62</sup>. (iii) MleP and MleS are more active at pH 6 (Figs. 1 and 2) than at pH 7 or higher, implying a built-in mechanism for pH homeostasis. Thus, more protons are taken up by the decarboxylation pathway when the internal pH decreases, e.g. as a result of a lower external pH or import of protons via secondary active transporters such as GltP and LacY. The relative simplicity and versatility of the pathway to generate a PMF and to maintain the internal pH relatively constant is an advantage for the further integration of metabolic modules in synthetic cells. Indeed, we show successful integration of the L-malate decarboxylation pathway with a metabolic network for the formation of precursors of the glycolytic (glucose-6P) and pentose phosphate pathway (6-phosphoglucono- $\delta$ -lactone) from the internalized lactose. The main function of the pentose phosphate pathway is to provide the cell with precursors for nucleotide synthesis and reducing power (NADPH)<sup>63</sup>. Hence, the here presented system constitutes a platform for the integration of other essential functions like redox or ATP/ADP homeostasis<sup>64,65</sup>.

What are the limitations of the L-malate decarboxylation pathway? First, L-lactic acid (present in low amounts at pH 7 but in rapid equilibrium with L-lactate) is highly membrane permeable<sup>66–68</sup>, which in our system results in competition between external L-lactic acid with L-malate. This reduces the exchange rate and, hence, limits the generation of PMF. Second, the decrease in activity in MleP and MleS at pH > 6 may impose a limit on the capacity of the L-malate decarboxylation pathway to generate a PMF at alkaline pH values.

The PMF in living cells fluctuates and responds to changes in the external medium<sup>69,70</sup>. PMF values in cells have been reported to fall within the range –100 to –270 mV, depending on the specific organism and conditions<sup>71</sup>. The PMF from the L-malate decarboxylation pathway in liposomes at pH 7 was maximally  $\approx$  –100 mV, i.e., 8 min after L-malate addition and reached  $\approx$  –120 mV after 12 min at pH 6 (Fig. 4d, e). Subsequently, the PMF decreased to  $\approx$  –70 mV at pH 7, mostly as a consequence of the partial dissipation of the membrane potential (Fig. 4d). Hence, at longer times, the contribution of  $\Delta$ pH to the PMF increased relative to that of the  $\Delta\Psi$ . We used in most of our studies a pH of 7; the PMF is higher at lower pH values reflecting the pH regulation of MleP and MleS.

The accumulation of L-glutamate and D-lactose nicely follows the transients in the PMF, suggesting the energy from the PMF is actively transformed into a substrate gradient by the symporters and, remarkably, we obtain H<sup>+</sup>/solute stoichiometries of –3 for GltP and –1 for LacY. These values nicely match the mechanistic stoichiometries of these proteins. In older literature, the relationship between the magnitude of the PMF and lactose accumulation has been found condition-dependent, which has led to the suggestion that the mechanistic stoichiometry of LacY (and other transporters) may vary. Our estimates match the mechanistic stoichiometry, which may be due to the fact that we work at relatively low PMF and close to pH 7, where leak pathways may be less prominent<sup>72,73</sup>.

The internal L-glutamate concentration reaches 1 mM, when the external concentration is only 20  $\mu$ M. For biosynthesis, the cellular amino acid concentrations are typically in the low millimolar range; the glutamate concentrations are typically higher because this amino acid also serves a role as compatible solute, and its oxidation

can feed oxidative phosphorylation with reducing equivalents for in vitro protein synthesis<sup>74–78</sup>. Reaching intravesicular concentrations in the GltP vesicles similar to those in *E. coli* would require an external concentration of L-glutamate of 0.6–0.8 mM. We also note that, at 20  $\mu$ M of L-glutamate, GltP operates at <40% of its maximal rate.

A reference value for the intracellular concentration of lactose is not available, because in cells the disaccharide is quickly broken down to galactose plus glucose, which are further metabolized via the Leloir and glycolytic pathway<sup>79</sup>, respectively. We have determined the uptake of lactose at an external concentration of 50  $\mu$ M, which is well below the  $K_m$  of LacY (0.5 mM, Table 1). Hence, a much faster uptake is feasible at higher substrate concentration. We also notice slow lactose efflux at higher internal lactose concentrations (at  $t > 2$  h, Fig. 6c), which is possibly linked with H<sup>+</sup>:lactose uncoupling events that are more prominent at alkaline pH values<sup>73,80</sup>. Indeed, uncoupling of solute-H<sup>+</sup> symport has been reported as strategy to prevent unconstrained accumulation of solutes<sup>81,82</sup>.

In summary: we show sustainable and long-term accumulation of an amino acid and metabolism of a sugar, driven by a PMF-generating pathway that could be implemented in various types of synthetic cells and used to sustain far-from-equilibrium metabolism. A synthetic cell requires 20 amino acids (but also other nutrients), which could be taken up by separate amino acid transporters. To limit the number of transporters to be reconstituted and later on to be produced by in-vesicle synthesis and membrane insertion, we envisage the use of a broad specificity di-/tripeptide transporter such as DtpT together with luminal peptidases to supply the cell with all amino acids<sup>41,83,84</sup>. Similarly, the integration of H<sup>+</sup>:ribonucleoside symporters along with ribonucleoside kinases or H<sup>+</sup>:nucleotide symporters can provide building blocks for the synthesis of DNA and RNA<sup>85,86</sup>. Co-constitution of the L-malate decarboxylation pathway along with Na<sup>+</sup>/H<sup>+</sup> antiporters is a strategy to fine-tune the pH homeostasis or convert the PMF into a SMF. This would extend the possibilities of building block carriers to symporters driven by a Na<sup>+</sup> electrochemical gradient, e.g., as present in mammalian cells. Given the importance of the PMF (and SMF) as energy carrier in all organisms from all kingdoms of life, the here-developed chemiosmotic network may inspire other studies of molecular and cellular processes that require electrochemical ion gradients.

## Methods

### Plasmid construction for the expression of MleP and MleS

The plasmids bearing the *mleP* and *mleS* genes were constructed following the method from<sup>87</sup> as follows: The *mleP* and *mleS* genes were amplified from the genome of *L. lactis* IL1403 by PCR with primers *mleP\_clic\_fw* and *mleP\_clic\_rev* for MleP, and *mleS\_clic\_fw* and *mleS\_clic\_rev* for MleS (Supplementary Table 2), using Phusion HF DNA polymerase (Thermo Fisher Scientific, Inc.). This yielded plasmids pNZ\_clic\_MleP and pNZ\_clic\_MleS. Both genes are under the nisin A-inducible  $P_{nis}$  promoter, and the proteins have a TEV cleavable 10 His-tag at the C-terminus. Both pNZ\_clic\_MleP and pNZ\_clic\_MleS were transformed into *L. lactis* NZ9000.

### Expression of *L. lactis* MleP and MleS

Expression of *L. lactis* MleP and MleS was performed in a batch culture as follows: *L. lactis* NZ9000 cells transformed with pNZ\_clic\_MleP or pNZ\_clic\_MleS were grown in 3 L of rich media (2% (w/v) Gistex, 65 mM sodium phosphate pH 7, 1% (w/v) glucose) supplemented with 5  $\mu$ g mL<sup>–1</sup> chloramphenicol at 30 °C (without stirring) after inoculation with 50 mL of an overnight pre-culture. At an optical density (OD<sub>600</sub>) of 0.5, the expression was induced with 0.05% (v/v) of culture supernatant from a nisin A-producing strain. The strains were grown for an additional 2 hours and then harvested by centrifugation (6000  $\times$  g, 4 °C, 15 minutes), washed once, resuspended in ice-cold 100 mM

potassium phosphate pH 7 to an  $OD_{600} \approx 100$ , frozen in liquid nitrogen, and stored at  $-80^\circ\text{C}$ .

### Expression of *E. coli* GltP

GltP was produced from plasmid pBad24-GltP. Expression was performed in *Escherichia coli* MC1061 cells, grown in LB broth at  $37^\circ\text{C}$  and shaken at 200 rpm. Ampicillin was added to the cultures to a final concentration of  $100\ \mu\text{g mL}^{-1}$ . At an optical density at 600 nm of 0.8–1.0, L-arabinose was added to a final concentration of 0.01% (w/v) and the temperature was switched to  $25^\circ\text{C}$ . Five hours after induction, the cells were harvested ( $6268 \times g$ , 10 min,  $4^\circ\text{C}$ , Beckman JLA 9.1000 rotor), washed once, and resuspended in ice-cold 20 mM Tris-HCl pH 8 to an  $OD_{600} \approx 150$ , frozen in liquid nitrogen, and stored at  $-80^\circ\text{C}$ .

### Expression of *E. coli* LacY

*E. coli* BL21 cells transformed with the plasmid pT7C3H-lacY (containing the coding region of LacY and the protein tagged with  $10\times$  His at the C-terminus) were grown in LB medium supplemented with  $100\ \mu\text{g mL}^{-1}$  of ampicillin at  $37^\circ\text{C}$  and stirring at 150 rpm. Induction of protein expression was performed at  $30^\circ\text{C}$  at an  $OD_{600}$  of 0.5 with 0.4 mM of isopropyl  $\beta$ -D-1-thiogalactopyranoside for a period of 3 h. Cells were harvested by centrifugation ( $6000 \times g$ ,  $4^\circ\text{C}$ , 15 minutes), washed once, resuspended in ice-cold 100 mM potassium phosphate pH 7 to an  $OD_{600} \approx 100$ , frozen in liquid nitrogen, and stored at  $-80^\circ\text{C}$ .

### Purification of *L. lactis* MleS

*L. lactis* cells overexpressing MleS were thawed and lysed at 30 kPsi in a high-pressure homogenizer (HPL6, Maximator) in the presence of  $100\ \mu\text{g mL}^{-1}$  DNase, 2 mM  $\text{MgSO}_4$  and 1 mM PMSF. After lysis, 5 mM of sodium-EDTA was added. Cell debris was removed by centrifugation (15 min,  $22,000 \times g$ ,  $4^\circ\text{C}$ ) and the supernatant was centrifuged for 90 min at  $125,000 \times g$  and  $4^\circ\text{C}$ . Protein concentration in the cell lysate was determined by the bicinchoninic acid assay (BCA) (ThermoFisher Scientific Protein Assay kit) using BSA as standard, the cell lysate was frozen in liquid nitrogen and stored at  $-80^\circ\text{C}$ .  $\text{Ni}^{2+}$ -Sephacryl resin (Cytiva) was washed with milliQ water and equilibrated with buffer A (200 mM NaCl, 50 mM potassium phosphate pH 7.5) plus 10 mM imidazole. Lysate was thawed on ice and incubated with  $\text{Ni}^{2+}$ -Sephacryl resin (0.5 ml column volume per 50 mg of total protein content) for 1 h with gentle mixing at  $4^\circ\text{C}$ . The suspension was transferred to a glass chromatography column (Bio-Rad). The resin was washed with 20 column volumes of buffer A plus 50 mM imidazole. Protein was eluted with buffer A containing 500 mM of Imidazole, and the protein concentration was determined from absorbance measurements at 280 nm using a Nanodrop™ (ThermoFisher Scientific). Fractions with the highest protein concentration were used for size-exclusion chromatography on a Superdex 200 Increase 10/300 GL column (GE Healthcare) in 100 mM NaCl, 50 mM potassium phosphate pH 7.0. Protein was supplemented with 10% glycerol, aliquoted, flash-frozen in liquid nitrogen, and stored at  $-80^\circ\text{C}$ .

### Purification of MleP and LacY

*L. lactis* cells overexpressing MleP or *E. coli* cells overexpressing LacY were thawed and lysed at 30 kPsi (*L. lactis*) or 20 kPsi (*E. coli*) in a high-pressure homogenizer (HPL6, Maximator) in the presence of  $100\ \mu\text{g mL}^{-1}$  DNase, 2 mM  $\text{MgSO}_4$  plus 1 mM PMSF. After lysis, 5 mM of sodium-EDTA was added. Cell debris was removed by centrifugation (15 min,  $22,000 \times g$ ,  $4^\circ\text{C}$ ) and the supernatant was centrifuged for 90 min at  $205,000 \times g$  and  $4^\circ\text{C}$ . Supernatant was discarded, and the pellet of cell membranes was resuspended in ice-cold potassium phosphate pH 7 to a total protein concentration of  $10\ \text{mg mL}^{-1}$  (Determined by the BCA assay). Resuspended membranes were flash-frozen in liquid nitrogen and stored at  $-80^\circ\text{C}$ . Membrane vesicles containing 20 mg of total protein were thawed on ice, and solubilized for one hour with *n*-dodecyl- $\beta$ -D-maltoside (DDM) [0.5% (w/v) for

MleP, 1.0% for LacY] in 200 mM NaCl, 50 mM potassium phosphate pH 7.5. Non-solubilized membranes were removed by centrifugation (25 min,  $270,000 \times g$ ,  $4^\circ\text{C}$ ).  $\text{Ni}^{2+}$ -Sephacryl resin (Cytiva) was washed with milliQ water, equilibrated with buffer A (200 mM NaCl, 50 mM potassium phosphate pH 7.5) supplemented with 10 mM imidazole plus 0.03% (for MleP) or 0.05% (for LacY) (w/v) of DDM and added to the solubilized membrane vesicles. The suspension was nutated for 1 h and subsequently transferred to a Poly-Prep chromatography column (Bio-Rad). The resin was washed with 20 column volumes of buffer A plus 50 mM imidazole and 0.03% (for MleP) or 0.05% (for LacY) (w/v) of DDM. Proteins were eluted with buffer A plus 350 mM imidazole and 0.03% (for MleP) or 0.05% (for LacY) (w/v) of DDM. Protein concentration was determined from absorbance measurements at 280 nm using a Nanodrop™ (ThermoFisher Scientific). 2 mM of  $\beta$ -mercaptoethanol was added to all the buffers for the purification of LacY.

### Purification of GltP

*E. coli* cells overexpressing GltP were thawed and lysed at 25 kPsi (*E. coli*) in a high-pressure homogenizer (HPL6, Maximator) in the presence of  $100\ \mu\text{g mL}^{-1}$  DNase, 2 mM  $\text{MgSO}_4$  plus 1 mM PMSF. Unbroken cells and cell debris were pelleted (30 min,  $12,074 \times g$ ,  $4^\circ\text{C}$ ), and the supernatant was subjected to ultracentrifugation (150 min,  $193,727 \times g$ ,  $4^\circ\text{C}$ ). Membrane pellets were resuspended in 20 mM Tris-HCl pH 8, and stored at  $-80^\circ\text{C}$ . The protein concentration in the membranes was determined using BCA method, with BSA as a standard. Proteins were solubilized from membrane vesicles in buffer B (300 mM NaCl, 50 mM HEPES pH 8.0), containing 15 mM imidazole pH 8.0 plus 1% *n*-decyl- $\beta$ -maltoside (w/v) (DM), at a final protein concentration of  $3\ \text{mg mL}^{-1}$ . After incubation on a rocking platform for 60 min, the solution was centrifuged (30 min,  $286,286 \times g$ ,  $4^\circ\text{C}$ ). Supernatants were incubated on a rotating platform for 60 min at  $4^\circ\text{C}$  with  $\text{Ni}^{2+}$ -Sephacryl slurry (Fast-flow, GE Healthcare, bed volume of 0.5 ml), pre-equilibrated with buffer A. The mixture was loaded on a BioRad Poly-Prep column, and unbound protein was allowed to flow through. Columns were washed with 20 column volumes of buffer C (500 mM KCl, 0.15% DM (w/v), 50 mM MES pH 6.0), supplemented with 150 mM imidazole pH 6.0 and continued washed with 5 column volumes of buffer C, supplemented with 200 mM imidazole pH 6.0. Protein was eluted from the column in three fractions of 350, 800, and 400  $\mu\text{L}$  using buffer C, supplemented with 500 mM imidazole pH 6.0. The second elution fraction from the affinity chromatography contained most of the purified protein. Protein concentration was determined from absorbance measurements at 280 nm using a Nanodrop™ (ThermoFisher Scientific).

### Lipid and vesicle preparation

*E. coli* polar lipids: egg PC (3:1). *E. coli* polar lipids were prepared by precipitation with acetone and then extraction with diethyl ether from a commercial extract of *E. coli* total lipids (Avanti Polar Lipids), according to ref. 88. *E. coli* polar lipids and egg PC (Avanti Polar Lipids) dissolved in chloroform were mixed to a molar ratio of 3:1.

DOPE:DOPG:DOPC (1:1:2). Synthetic lipids 1,2-dioleoyl-sn-glycero-3-phosphoethanolamine (DOPE), 1,2-dioleoyl-sn-glycero-3-phospho-(1'-rac-glycerol) (DOPG) and 1,2-dioleoyl-sn-glycero-3-phosphocholine (DOPC) (Avanti Polar Lipids) were dissolved in chloroform to a concentration of  $25\ \text{mg mL}^{-1}$  and mixed in a molar ratio of 1:1:2.

For the formation of vesicles (liposomes), the chloroform in the lipid mixtures was evaporated in a rotary evaporator (Büchi Labor-technik AG), the lipids were washed with diethyl ether, and the lipid film was hydrated and resuspended in 50 mM K-phosphate at pH 7 to a concentration of  $20\ \text{mg mL}^{-1}$ . Lipid resuspension was facilitated by sonication with a tip sonicator at 70% amplitude, 15 s ON, 45 s OFF for 16 cycles, while the suspension was kept cold in ice-water and subjected to three cycles of freezing (in liquid nitrogen)–thawing (in a water bath at room temperature). Large-unilamellar vesicles (LUVs)

were formed by extrusion of the lipid suspension through a 400 nm pore-size polycarbonate filter (Whatman, GE Healthcare).

### Reconstitution of membrane proteins

**Reconstitution mediated by Triton X-100 and detergent removal with polystyrene beads (MleP, GltP, and MleP plus GltP).** The protocol was adapted from ref. 89. Briefly, an aliquot (1 mL) of 20 mg mL<sup>-1</sup> of a mixture *E. coli* polar lipids:egg phosphatidylcholine (PC) 3:1 (mol ratio) or DOPE:DOPG:DOPC 1:1:2 (mol ratio) lipids were resuspended in 50 mM potassium phosphate pH 7.0 and 13× extruded through a 400 nm polycarbonate filter (Whatman, GE Healthcare) to form LUVs, diluted to a lipid concentration 4 mg mL<sup>-1</sup> in 50 mM potassium phosphate pH 7.0, and destabilized with 10% Triton X-100 by titration to OD<sub>540</sub> = 0.6 × R<sub>sat</sub> (R<sub>sat</sub> is point of maximal OD<sub>540</sub>). Detergent-purified membrane protein (≈1 mg mL<sup>-1</sup>) was added to the lipid-Triton X-100 mixture at the desired LPR ratio (w/w), and the protein-detergent-lipid mixture was incubated at room temperature for 30 min with gentle agitation. Detergent was removed by consecutive additions of polystyrene beads (BioBeads SM-2, BioRad) with continuous and gentle agitation as follows: 25 mg mL<sup>-1</sup> of polystyrene beads were added and incubated for 30 min at room temperature. A second portion of 15 mg mL<sup>-1</sup> was added and incubated for 60 min at 4 °C. A third portion of 20 mg mL<sup>-1</sup> was added and incubated overnight at 4 °C. After the last addition of 40 mg mL<sup>-1</sup> the mixture was incubated for 2 h at 4 °C. Polystyrene beads were discarded, proteoliposomes were harvested by centrifugation (25 min, 270,000 × g, 4 °C) and resuspended to a lipid concentration of 50 mg mL<sup>-1</sup> in 50 mM potassium phosphate pH 7.0.

**Reconstitution mediated by n-octyl-β-D-glucopyranoside (OG) and rapid dilution (MleP, LacY and MleP plus LacY).** The protocol was adapted from refs. 42–44. Briefly, 1 mL of 20 mg mL<sup>-1</sup> of *E. coli* polar: egg PC 3:1 (mol ratio) lipids were resuspended in 50 mM potassium phosphate pH 7.0 plus 1 mM dithiothreitol (DTT) and dissolved by adding OG to a final concentration of 1.8% (w/v) and incubation at room temperature for 2 h with agitation. DDM-purified membrane protein (≈1 mg mL<sup>-1</sup>) was added, and the mixture was incubated on ice for 10 min. The protein-detergent-lipid mixture was diluted at least 100× in ice-cold 50 mM potassium phosphate pH 7.0 plus 1 mM DTT, and the proteoliposomes were harvested by centrifugation (120 min, 205,000 × g, 4 °C). The pellet was resuspended in 50 mM potassium phosphate pH 7.0 plus 1 mM DTT to a lipid concentration of 10 mg mL<sup>-1</sup>, polystyrene beads (BioBeads SM-2, BioRad) were added (50 mg mL<sup>-1</sup>), and the mixture was incubated overnight at 4 °C with gentle agitation. Polystyrene beads were discarded, proteoliposomes were harvested by centrifugation (25 min, 270,000 × g, 4 °C) and resuspended to a lipid concentration of 50 mg mL<sup>-1</sup> in 50 mM potassium phosphate pH 7.0 plus 1 mM DTT.

MleP LPR 100 vesicles composed of *E. coli* polar lipids: egg PC 3:1 (mol ratio) was the standard for the characterization of MleP by SSM measurements. This LPR yields about 60 MleP molecules per vesicle of diameter 200 nm, which is sufficient for large and robust electrical signals even at very low concentrations of substrate. Previous studies have shown that the reconstitution efficiency decreases with decreasing LPR<sup>37,38</sup>. Hence, we increased the LPR to 250 for experiments when multiple membrane proteins had to be reconstituted (MleP with GltP or LacY) and MleS was encapsulated. We tested two different lipid compositions to demonstrate that, besides *E. coli* polar lipids+egg PC (3:1), MleP also functions in synthetic lipid mixtures like DOPE:DOPG:DOPC (1:1:2) (Fig. 1f and Supplementary Fig. 2), albeit less efficiently (Supplementary Fig. 2).

### SSM-based electrophysiological measurements

Liposomes or proteoliposomes were adsorbed onto an SSM performed on a gold sensor chip and transport currents were detected via

capacitive coupling, as explained elsewhere<sup>28,29</sup>. Proteoliposomes with MleP in *E. coli* polar: egg PC lipids 3:1 (mol ratio) at the indicated LPR (w/w) were used for the encapsulation of sodium-L-lactate or sodium-L-malate in 100 mM potassium phosphate pH 7.0 by 5× freeze-thaw cycles (flash-freezing in liquid nitrogen, thawing in an ice-water bath at ≈10 °C), followed by gentle mixing and 13× extrusion through a 200 nm polycarbonate filter (Whatman, GE Healthcare). Extruded proteoliposomes were collected by centrifugation (25 min, 270,000 × g, 4 °C) and resuspended to a final lipid concentration of 5 mg mL<sup>-1</sup> in non-activating (NA) solution (see below) containing either L-malate or L-lactate.

10 μL of MleP proteoliposomes were applied onto an SSM, performed on an octadecanethiol-functionalized gold sensor chip (3 mm diameter, Nanion) by the addition of 1,2-diphytanoyl PC (15 mg mL<sup>-1</sup> in *n*-decane) (Avanti Polar Lipids) and NA solution (see below). The adsorption of proteoliposomes to the SSM was accelerated by centrifugation of the sensor chip at 2500 × g, 30 min at room temperature. The sensor chip with the proteoliposomes adsorbed on the SSM were loaded into the chamber of a SURFE2R N1 device (Nanion) and a jump in the concentration of substrate was triggered via a software-controlled fast solution exchange protocol<sup>29</sup> at room temperature.

The solution exchange protocol consisted of an initial perfusion of NA solution for 1 sec followed by the perfusion of activating solution (A) for 1 sec and a final perfusion of NA solution for 1 sec. The A solution contained the substrate that initiates the transport. The composition of the NA solution was the same as that in the lumen of the proteoliposomes. Current signals obtained during the perfusion of A solution were taken for quantification purposes (ON signals). For all the measurements, we used 100 mM potassium phosphate at the indicated pH. Ionic strength and osmolarity were made similar for the A and NA solutions; acetate<sup>-</sup> and sulfate<sup>2-</sup> were used as non-transported anions to replace L-lactate<sup>-</sup> and L-malate<sup>2-</sup>, respectively. For pH dependence, proteoliposomes adsorbed onto the SSM were incubated for 20 min in NA solution at the corresponding pH before the solution exchange for pH equilibration. Supplementary Table 3 summarizes the transport modes and conditions of the solution exchange.

For the L-malate dependence, the A solution was x mM Na-L-malate, (30-x) mM Na-sulfate plus 30 mM Na-acetate, while the NA solution was 30 mM Na-L-lactate plus 30 mM of Na-sulfate. For the L-lactate dependence, the A solution was x mM Na-L-lactate, (30-x) mM Na-acetate plus 30 mM Na-sulfate, while the NA solution was 30 mM Na-L-malate plus 30 mM of Na-acetate.

### L-malate efflux assays

For the efflux assays 20 mg of MleP proteoliposomes (lipid-to-protein ratio 400:1) were used. The vesicles were extruded 13 times through a 200 nm pore-size polycarbonate filter, diluted to 6 mL in 100 mM potassium phosphate pH 7.0, and collected by centrifugation (25 min, 270,000 × g, 4 °C). The vesicles were resuspended in as little solution as possible (<100 μL). To load the vesicles with substrate, 1 mM of <sup>14</sup>C-L-malate was added (final specific activity: 600 MBq mmol<sup>-1</sup>). This suspension was incubated at room temperature for 1 hour, followed by overnight incubation at 4 °C. The vesicles were diluted to a final concentration of 3.34 mg of lipid mL<sup>-1</sup> in 100 mM potassium phosphate pH 7.0 or sodium phosphate pH 7.0. Next, 0.2 μM valinomycin (stock solution of 100 μM in ethanol) was added to either dissipate any formed membrane potential, or to create a membrane potential (inside negative) in vesicles resuspended in sodium phosphate buffer. 100 μL samples were taken at given time intervals, diluted in 2 mL of ice-cold quenching buffer (100 mM potassium phosphate pH 7.0), and filtered over 0.45 μm pore size cellulose nitrate filters. The filters were washed with 2 mL quenching buffer. Radioactivity was quantified by liquid scintillation counting using Ultima Gold MV scintillation fluid (PerkinElmer) and a Tri-Carb 2800TR scintillation counter (PerkinElmer).

### MleS activity assay

L-malate decarboxylation activity catalyzed by MleS was estimated from the H<sup>+</sup> consumption with a pH combination microelectrode (BlueLine 16, SI Analytics) in a solution with low buffer capacity. 700  $\mu\text{L}$  of reaction solution containing 0.5 mM NAD<sup>+</sup>, 0.1 mM MnCl<sub>2</sub>, 100 mM KCl, and 2 mM potassium phosphate at pH 7.0 were incubated for 3 min at 30 °C. The enzyme was added at the concentration indicated in Fig. 2 (50–150 nM), and a temperature equilibration step of 3 min was performed. The decarboxylation reaction was initiated ( $t=0$ ) by the addition of sodium-L-malate to a final concentration of 5 mM (or otherwise indicated) from a stock solution whose pH was adjusted to pH 7.0 with NaOH. For the pH dependence, 2 mM potassium phosphate was used at pH 6–8, while sodium-acetate was used for experiments at pH 4 and 5, keeping the L-malate concentration at 5 mM and MleS concentration at 150 nM. For the L-malate dependence, the enzyme concentration was 150 nM. The L-malate decarboxylation activity was calculated as the H<sup>+</sup> consumption expressed in  $\mu\text{mol H}^+ \text{min}^{-1} \text{mg}^{-1}$ , using a titration curve with NaOH to calibrate the buffer capacity. The pH was recorded during the progression of the reaction with the software MultiLab Pilot V5.21 (Xylem Inc.).

### Encapsulation of soluble components of the L-malate decarboxylation

The protocol was adapted from<sup>65</sup>. 2 mM sodium-L-lactate, 1.0 mM sodium- $\beta$ -nicotinamide adenine dinucleotide (NAD<sup>+</sup>), 0.5 mM MnCl<sub>2</sub>, 0.1 mM HPTS, pyranine, (ThermoScientific), and 2.5  $\mu\text{M}$  MleS was mixed with 10 mg of proteoliposomes resuspended to a lipid concentration of 25 mg mL<sup>-1</sup> in 50 mM potassium phosphate pH 7 to a final volume of 400  $\mu\text{L}$ . Encapsulation of soluble components was performed by a 5 $\times$  freeze-thaw cycle (flash-freezing in liquid nitrogen, and thawing in an ice-water bath at  $\approx 10$  °C) followed by gentle mixing and 13 $\times$  extrusion through a 400 nm polycarbonate filter (Whatman, GE Healthcare). External components were removed by gel filtration on a 22 cm long column with Sephadex G-75 (Sigma) pre-equilibrated with 2 mM sodium-L-lactate plus 50 mM potassium phosphate pH 7.0. Proteoliposomes were washed twice with 60 $\times$  volume dilution, followed by centrifugation (25 min, 270,000  $\times g$ , 4 °C) and resuspension to a final lipid concentration of 125 mg mL<sup>-1</sup>. 2 mM of DTT was added to all buffers when vesicles with LacY were used.

### Internal pH measurements

The internal pH of the vesicles was determined from fluorescence of encapsulated pyranine (trisodium-8-hydroxypyrene-1,3,6-trisulfonate, HPTS (ThermoFisher Scientific))<sup>90</sup>. Pyranine was encapsulated in proteoliposomes (along with the soluble components of the L-malate decarboxylation pathway) at a concentration of 0.1 mM, as described in the previous section. Liposomes or proteoliposomes containing internal pyranine were diluted 50 times in an external solution (2 mM sodium-L-lactate plus 50 mM potassium phosphate pH 7, unless otherwise indicated) to a lipid concentration of 2.5 mg mL<sup>-1</sup> in a quartz fluorescence cuvette (105.250 QS, Hellma Analytics). To eliminate the fluorescence from traces of pyranine on the outside, 5 mM of the collisional quencher *p*-xylene-bispyridinium bromide (DPX) was included in the external solution. The mixture was incubated for 10 min at 30 °C, and the L-malate decarboxylation reaction started by the addition of 10 mM (unless otherwise indicated) of sodium-L-malate (from a 2 M stock pre-adjusted to pH 7 with NaOH). Where the effect of ionophores was to be determined, valinomycin and nigericin dissolved in dimethyl sulfoxide (DMSO) were added to a concentration of 1  $\mu\text{M}$  (lipid:ionophore  $\approx 3000:1$  (mol ratio)). Fluorescence measurements were performed in an FP-8300 spectrofluorometer (Jasco, Inc). Excitation spectra of pyranine between 380 and 480 nm ( $\lambda_{\text{exc}}$ ) at an emission wavelength ( $\lambda_{\text{em}}$ ) of 512 nm were taken at intervals of 1 min. The ratio between the fluorescence intensities at  $\lambda_{\text{exc}} = 450$  nm and 405 nm

( $F_{450\text{nm}}/F_{405\text{nm}}$ ) was calculated and interpolated in a calibration curve to obtain the pH values. For the calibration curve: Pyranine was diluted 1000 times in the solution of 50 mM potassium phosphate at the indicated pH to a final concentration of 0.1  $\mu\text{M}$ , and the excitation spectra were measured as described above. The pH of the buffer was measured right before starting the fluorescence measurements with a pH microelectrode.  $F_{450\text{nm}}/F_{405\text{nm}}$  was plotted against the measured pH (Supplementary Fig. 10c), and the data were fitted to a logistic equation of the form:

$$y = \frac{a}{1 + e^{-k(x-x_c)}} \quad (4)$$

Where  $y = F_{450}/F_{405}$ ,  $x = \text{pH}$ ,  $a = 3.741$ ,  $k = 2.223$  and  $x_c = 7.883$ . To calculate the pH from the fluorescence excitation spectra of pyranine we used the following equation:

$$\text{pH} = 7.883 - \frac{1}{2.223} \ln \left( \frac{3.741}{(F_{450}/F_{405})} - 1 \right) \quad (5)$$

### L-lactate quantification by RP-HPLC

**MleS activity in solution.** To measure L-lactate production by MleS in solution, the enzyme was diluted to a concentration of 50 nM in 0.5 mM NAD<sup>+</sup>, 0.1 mM MnCl<sub>2</sub>, 100 mM KCl plus 2 mM potassium phosphate pH 7.0 and incubated at 30 °C for 3 min. The reaction was initiated by the addition of 5 mM sodium-L-malate (pre-adjusted to pH 7 with NaOH). 50  $\mu\text{L}$  aliquots were taken at 0 s, 10 s, 30 s, 60 s, 2 min, 3 min, 5 min, 10 min, 20 min, and 30 min, and processed as described below.

**Production of L-lactate by the L-malate decarboxylation pathway in vesicles.** MleP-proteoliposomes containing 2 mM sodium-L-lactate, 1.0 mM NAD<sup>+</sup>, 0.5 mM MnCl<sub>2</sub> plus 50 mM potassium phosphate pH 7.0 were diluted 50 times in external solution containing 2 mM sodium-L-lactate and 50 mM potassium phosphate pH 7.0 and incubated at 30 °C for 3 min. The L-malate decarboxylation pathway was initiated by the addition of 10 mM sodium-L-malate (from a 2 M stock pre-adjusted to pH 7 with NaOH), and 50  $\mu\text{L}$  aliquots were taken at the indicated times over a period of 4 hours and processed as described below. A sample before the addition of L-malate was also taken.

**Derivatization and analysis.** The protocol for the analysis of L-lactate was adapted from ref. 91. L-malate decarboxylation in solution or in MleP-proteoliposomes was stopped by transferring 50  $\mu\text{L}$  of samples into 20  $\mu\text{L}$  of quenching solution (7% perchloric acid plus 4.5 mM EDTA). The excess acid was neutralized by the addition of 15  $\mu\text{L}$  of 1 M KOH plus 1 M KHCO<sub>3</sub>, and samples were incubated overnight at -20 °C. Samples were centrifuged at 16,000  $\times g$  for 5 min at room temperature in a table top centrifuge and 10  $\mu\text{L}$  of the supernatant was transferred to 20  $\mu\text{L}$  of 5% (w/v) triethanolamine (TEA) in acetonitrile (ACN) plus 90  $\mu\text{L}$  of 90 mM tetra-*n*-butylammonium bromide in acetonitrile. 380  $\mu\text{L}$  of derivatization reagent (10 mM 9-chloromethyl anthracene (9-CMA, ThermoFisher Scientific) in acetonitrile) was added, and the reaction was run at 70 °C for 30 min. The solution 9-CMA was previously sonicated in a water bath for 15 min and filtrated through a PTFE filter. Derivatized samples at room temperature were centrifuged for 5 min at 16,000  $\times g$  and 10  $\mu\text{L}$  of a 2 $\times$  diluted supernatant was analyzed by RP-HPLC on a 1260 LC HPLC system (Agilent) composed of a G1311B binary pump, G1329B autosampler, G1316A thermostated column compartment and a G1315C diode array detector, using a Shimadzu XR-ODS 3  $\times$  75 mm C18 column. Samples were run with a binary gradient between ACN and water as follows: start was at 30% ACN, 80% ACN at 10 min, 95% ACN from 11 to 15 min, 30% ACN from 16 min to the

end (20 min), flow rate  $0.9 \mu\text{L min}^{-1}$ . The column was kept at  $40^\circ\text{C}$ , while samples in the autosampler were kept at  $10^\circ\text{C}$ . Samples were analyzed by detection of absorbance at  $365 \text{ nm}$ . L-lactate derivative was detected based on the retention time and quantified by interpolation of the peak area from a calibration curve (Supplementary Fig. 6).

### Determination of membrane potential in vesicles

The membrane potential in liposomes and proteoliposomes was estimated using 3,3'-dipropylthiadicarbocyanine iodide ( $\text{DiSC}_3(5)$ , Invitrogen) as a fluorescent probe.

**Membrane potential in vesicles with the L-malate decarboxylation pathway.** MleP at LPR 250 (w/w) in *E. coli* polar lipids:egg PC 3:1 (mol ratio) liposomes containing  $2.5 \mu\text{M}$  MleS,  $1 \text{ mM}$   $\text{NAD}^+$ ,  $0.5 \text{ mM}$   $\text{MnCl}_2$ ,  $2 \text{ mM}$  sodium-L-lactate, ( $\pm 0.1 \text{ mM}$  pyranine) plus  $50 \text{ mM}$  potassium phosphate pH 7.0 were diluted 650 times in  $0.98 \text{ mL}$  of  $2 \text{ mM}$  sodium-L-lactate (unless otherwise indicated) plus  $50 \text{ mM}$  potassium phosphate pH 7.0 to a final concentration of lipids of  $0.2 \text{ mg mL}^{-1}$  in a cuvette for fluorescence measurements. The suspension was incubated at  $30^\circ\text{C}$  for 3 min with constant stirring ( $700 \text{ rpm}$ ) using a glass-covered magnetic bar.  $\text{DiSC}_3(5)$  was added to a final concentration of  $1 \mu\text{M}$  from a  $1 \text{ mM}$  stock in DMSO. After an equilibration time of 5 min, L-malate decarboxylation was initiated by addition of  $10 \text{ mM}$  sodium-L-malate (from a  $2 \text{ M}$  stock pre-adjusted to pH 7.0 with NaOH) and the fluorescence quenching ( $F_q$ ) was followed for 30–60 min. Valinomycin was added to a final concentration of  $50 \text{ nM}$  from a  $50 \mu\text{M}$  stock in DMSO to dissipate the membrane potential, which is observed as an increment in fluorescence ( $F_{\text{val}}$ ). The percentage of fluorescence quenching ( $\Delta F\%$ ) was calculated according to Eq. (6) and interpolated in a calibration curve (obtained for the same liposome samples) to estimate the magnitude of the L-malate-induced membrane potential.

$$\Delta F(\%) = \frac{F_q - F_{\text{val}}}{F_{\text{val}}} \quad (6)$$

**Calibration curve.** MleP at LPR 250 (w/w) in *E. coli* polar lipids:egg PC liposomes containing  $50 \text{ mM}$  of potassium phosphate pH 7.0 were 650 times diluted in  $0.98 \text{ mL}$  of  $50 \text{ mM}$  potassium phosphate,  $50 \text{ mM}$  sodium phosphate or mixtures of these buffers to obtain the desired  $\text{K}^+$  concentration on outside of the vesicles (Supplementary Table 4).  $\text{DiSC}_3(5)$  was added to a final concentration of  $1 \mu\text{M}$  from a  $1 \text{ mM}$  stock in DMSO and, after equilibration, valinomycin was added to a final concentration of  $50 \text{ nM}$  from a  $50 \mu\text{M}$  stock in DMSO. As a response to the negative inside membrane potential established from the diffusion of  $\text{K}^+$  along its concentration gradient, the fluorescence was quenched to a final level ( $F_q$ ) depending on the magnitude of the  $\text{K}^+$  gradient. Nigericin was added in order to dissipate the membrane potential causing a fluorescence dequenching ( $F_{\text{Nig}}$ ). The calibration curve was constructed by plotting the percentage of quenching (Fluorescence quenching %), calculated according to Eq. (7) and using the imposed potassium diffusion potential.

$$\Delta F(\%) = \frac{F_q - F_{\text{Nig}}}{F_{\text{Nig}}} \quad (7)$$

The  $\text{K}^+$  diffusion potential was calculated according to Eq. (8),

$$\Delta\Psi = 2.303 \left( \frac{RT}{F} \right) \log \left( \frac{[\text{K}^+]_{\text{OUT}}}{[\text{K}^+]_{\text{IN}}} \right) \quad (8)$$

where  $R$  is the gas constant,  $T$  is the temperature in Kelvin, and  $F$  is the Faraday constant. Data were fitted to an exponential equation (Supplementary Fig. 16b). The membrane potential was calculated from

fluorescence quenching curves using Eq. (9),

$$\Delta\Psi(\text{mV}) = k \ln \left( \frac{\Delta F(\%) - y_0}{A} \right) \quad (9)$$

where  $A = 30.7$ ,  $k = 108.4$ ,  $y_0 = -30.9$  are fitting parameters of the data in Supplementary Fig. 16b, and  $\Delta F(\%)$  corresponds to the fluorescence quenching.

Fluorescence measurements were performed in an FP8300 spectrofluorometer (JASCO) using a  $10 \times 4 \text{ mm}$  QS cuvette (Hellma Analytics, 109.004 F) at a temperature of  $30^\circ\text{C}$  under constant stirring ( $700 \text{ rpm}$ ) with a glass-covered magnetic bar. Excitation and emission wavelengths were  $662$  and  $680 \text{ nm}$ , respectively.

### Quantification of L-glutamate and D-lactose uptake in proteoliposomes

Proteoliposomes with MleP, GltP, or LacY containing the soluble components of the L-malate decarboxylation pathway ( $2 \text{ mM}$  sodium-L-lactate,  $1.0 \text{ mM}$   $\text{NAD}^+$ ,  $0.5 \text{ mM}$   $\text{MnCl}_2$  plus  $50 \text{ mM}$  potassium phosphate pH 7.0) were 50 times diluted in external solution containing  $2 \text{ mM}$  sodium-L-lactate,  $50 \text{ mM}$  potassium phosphate pH 7.0 and  $20 \mu\text{M}$  of  $^{14}\text{C}$ -radiolabelled sodium-L-glutamate (Perkin Elmer) (specific activity  $15 \text{ mCi/mmol}$ ,  $555 \text{ MBq/mmol}$ ) for GltP or  $50 \mu\text{M}$  of  $^{14}\text{C}$ -radiolabelled D-lactose (Amersham) (specific activity  $15.4 \text{ mCi/mmol}$ ,  $570.4 \text{ MBq/mmol}$ ) for LacY and incubated for 5 min at  $30^\circ\text{C}$  with continuous stirring.  $10 \text{ mM}$  of sodium-L-malate was added (from a  $1 \text{ M}$  stock adjusted to pH 7 with NaOH) to start the L-malate decarboxylation.  $100 \mu\text{L}$  samples were taken at indicated times before and after the addition of L-malate for up to 4 hours, diluted into  $2 \text{ mL}$  of ice-cold quenching solution ( $0.1 \text{ M}$  LiCl), and filtered over  $0.45 \mu\text{m}$  pore size nitrocellulose filters to stop the transport. The filter was washed, and radioactivity was quantified by liquid scintillation counting using Ultima Gold MV scintillation fluid (PerkinElmer) and a Tri-Carb 2800TR scintillation counter (PerkinElmer). As an alternative protocol, proteoliposomes were diluted in an external solution without substrate, and the radiolabelled substrate was added 30 min after the addition of L-malate; here, the L-glutamate or D-lactose transport is initiated after the generation of the PMF. When the effect of membrane potential or pH gradient dissipation was to be evaluated, valinomycin or nigericin was added to a final concentration of  $1 \mu\text{M}$  from a  $1 \text{ mM}$  stock in DMSO.

To determine the L-glutamate and D-lactose transport driven by the  $\Delta\Psi$  and  $\Delta\text{pH}$  from valinomycin-facilitated  $\text{K}^+$  diffusion and acetic acid diffusion potentials, respectively, the corresponding proteoliposomes (MleP plus GltP or MleP plus LacY) were loaded with  $2 \text{ mM}$  sodium-L-lactate,  $70 \text{ mM}$  potassium acetate and  $25 \text{ mM}$  of potassium phosphate at pH 7.0. The external composition was  $2 \text{ mM}$  sodium-L-lactate,  $22 \text{ mM}$  sodium acetate,  $25 \text{ mM}$  sodium phosphate pH 7.0,  $20 \mu\text{M}$  of radiolabelled L-glutamate for GltP (or  $50 \mu\text{M}$  of radiolabelled D-lactose for LacY),  $1 \mu\text{M}$  of valinomycin and different ratios of potassium-D-gluconate and sodium-D-gluconate to establish an outward  $\text{K}^+$  concentration gradient, according to Table 3. In this manner, the internal concentrations of  $\text{K}^+$  ( $[\text{K}^+]_{\text{IN}}$ ) and acetate ( $[\text{AcO}^-]_{\text{IN}}$ ) are  $109 \text{ mM}$  and  $70 \text{ mM}$ , respectively. The transport was initiated by a 50-fold dilution of proteoliposomes into the external solution (pre-incubated for 3 min at  $30^\circ\text{C}$ ).  $100 \mu\text{L}$  samples were taken at the indicated time intervals and processed as described above for quantification of radioactivity.

The driving forces from the pH gradient and membrane potential were calculated, using Eqs. (10) and (8), respectively.

$$\Delta\text{pH} = 2.303 \left( \frac{RT}{F} \right) \log \left( \frac{[\text{AcO}^-]_{\text{IN}}}{[\text{AcO}^-]_{\text{OUT}}} \right) \quad (10)$$

**Table 3 | Composition of external solutions for the simultaneous generation of membrane potential and pH gradient as driving forces for the uptake of L-glutamate or D-lactose**

External component*	ZΔpH (mV)** ≈ -30 ΔΨ (mV) = 0 (no valinomycin)	ZΔpH (mV) ≈ -30 ΔΨ (mV) = -25	ZΔpH (mV) ≈ -30 ΔΨ (mV) = -53	ZΔpH (mV) ≈ -30 ΔΨ (mV) = -75	ZΔpH (mV) = 30 ΔΨ (mV) = -103
Na-acetate (mM)	22	22	22	22	22
Na-D-gluconate (mM)	48	8	36	44	48
K-D-gluconate (mM)	0	40	12	4	0
[K <sup>+</sup> ] <sub>o</sub> ***	2.2	42.2	14.2	6.2	2.2

\*In addition to 2 mM sodium-L-lactate, 25 mM sodium phosphate pH 7.0, the radiolabelled substrate with/without 1 μM valinomycin. \*\* With this gradient of acetate, the ΔpH = 0.5. \*\*\*Calculated from the addition of potassium-D-gluconate plus K<sup>+</sup> contribution from the dilution of proteoliposomes in external solution (2.2 mM).

### Fluorometric determination of lactose metabolism in vesicles

**Enzymes.** β-galactosidase (LacZ) from *E. coli* (Sigma, G5635, lyophilized) was hydrated in 50 mM K-phosphate pH 7, 5 mM β-mercaptoethanol, 10 mM MgCl<sub>2</sub> plus 10% glycerol to a final concentration of 10 mg mL<sup>-1</sup> on ice until a translucent solution was obtained. Hexokinase (HK) from yeast (Roche, I1426365001) and glucose-6-phosphate dehydrogenase (G6P-DH) from yeast (Sigma, G7877) were acquired as suspensions in 3.2 M of ammonium sulfate. An aliquot of every resuspension was centrifuged at 15,000 × g for 10 min at 4 °C, and the supernatant was discarded. The pellet was dissolved in 50 mM K-phosphate pH 7, 5 mM β-mercaptoethanol, 10 mM MgCl<sub>2</sub> plus 10% glycerol to a final concentration of 8.5 mg mL<sup>-1</sup> (HK) and 15 mg mL<sup>-1</sup> (G6P-DH). Protein concentration was determined from absorbance measurements at 280 nm using a Nanodrop™ (ThermoFisher Scientific).

**Encapsulation.** Soluble components of the L-malate decarboxylation pathway (2.5 μM MleS, 1 mM NAD<sup>+</sup>, 0.5 mM MnCl<sub>2</sub> plus 2 mM Na-lactate) along with 7 μM β-galactosidase, 7 μM hexokinase, 4 μM G6P-DH, 10 mM MgATP, 2 mM NADP<sup>+</sup> were encapsulated in MleP LPR 250 (w/w)-LacY LPR 200 (w/w) or MleP LPR 250 vesicles with *E. coli* polar lipids: egg PC 3:1 (mol ratio) via OG-mediated reconstitution and detergent removal by rapid dilution<sup>42,43</sup>. Encapsulation, washing and resuspension was performed according to the protocol described in “Encapsulation of soluble components of the L-malate decarboxylation”.

**NADPH fluorescence measurements.** Proteoliposomes with encapsulated components were diluted 40× in 50 mM K-phosphate pH 7, Na-lactate 2 mM, 1 mM DTT plus 2.5 mM EDTA, unless otherwise indicated, and the suspension was incubated for 5 min at 30 °C. 10 mM of Na-malate was added from a 1 M stock and the mixture was incubated for 30 min to pre-form a PMF from the L-malate decarboxylation pathway. Then, D-lactose was added to a final concentration of 100 μM from a 4 mM stock (40× dilution). For inhibition of lactose transport, TMG or TDG were added to a final concentration of 20 mM before the addition of D-lactose. Fluorescence measurements were performed in a FP-8300 spectrofluorometer (Jasco, Inc). Emission spectra of NADPH between 380 and 500 nm (λ<sub>em</sub>) at an excitation wavelength (λ<sub>exc</sub>) of 350 nm were taken at intervals of 1 min during the whole experiment.

### Statistics and reproducibility

Uncropped gels for the images presented in Figs. 1a, 2b, 3b, 5b, 6b can be found in Supplementary Figs. 1 and 9 and as Source Data. The band patterns observed in the SDS-polyacrylamide gels are representative from at least two independent experiments (different sample preparations). In Supplementary Fig. 1a, c, three and two independent uncropped gels are presented for the analysis of MleP and LacY in liposomes, respectively, showing that images in Figs. 1a and 6b are representative from independent sample preparations. Lanes 7 and 8 in Supplementary Fig. 1b and Lanes 8 and 9 in Supplementary Fig. 9 correspond to independent reconstitution samples and show that images in Figs. 5b and 3b are representative of independent preparations.

Independent replicates with different sample preparations are indicated by *n* number in the Figure legends, and the standard deviation (SD) is indicated when *n* > 2.

### Data analysis and figures design

Data and statistical analysis were performed using OriginPro Lab v8.5. Cartoons in Fig. 1b, g, 2a, 3a, 4a, 5a, e, 6a, d. were created with Biorender.com released under a Creative Commons Attribution-NonCommercial-NoDerivs 4.0 International license. Figures were designed with Adobe Illustrator.

### Reporting summary

Further information on research design is available in the Nature Portfolio Reporting Summary linked to this article.

### Data availability

All data in this study are available within the main text, Supplementary Information and Source Data files. Source data is available for Figs. 1–6, Supplementary Figs. 1–3 and 5–27, Table 1 and Supplementary Table 1 in the associated source data file. Source data are provided with this paper.

### References

- Konings, W. N., Poolman, B. & van Veen, H. W. Solute transport and energy transduction in bacteria. *Antonie Van Leeuwenhoek* **65**, 369–380 (1994).
- Mitchell, P. Chemiosmotic coupling in oxidative and photosynthetic phosphorylation. *Biol. Rev. Camb. Philos. Soc.* **41**, 445–502, (1966).
- Konings, W. N. The cell membrane and the struggle for life of lactic acid bacteria. *Antonie Van Leeuwenhoek* **82**, 3–27 (2002).
- Konings, W. N., Poolman, B. & Driessen, A. J. Bioenergetics and solute transport in lactococci. *Crit. Rev. Microbiol.* **16**, 419–476 (1989).
- Konings, W. N. et al. The role of transport processes in survival of lactic acid bacteria. Energy transduction and multidrug resistance. *Antonie Van Leeuwenhoek* **71**, 117–128 (1997).
- Dimroth, P. & Schink, B. Energy conservation in the decarboxylation of dicarboxylic acids by fermenting bacteria. *Arch. Microbiol.* **170**, 69–77 (1998).
- Poolman, B. et al. Malolactic fermentation: electrogenic malate uptake and malate/lactate antiport generate metabolic energy. *J. Bacteriol.* **173**, 6030–6037 (1991).
- Renault, P., Gaillardin, C. & Heslot, H. Role of malolactic fermentation in lactic acid bacteria. *Biochimie* **70**, 375–379 (1988).
- Lolkema, J. S., Poolman, B. & Konings, W. N. Role of scalar protons in metabolic energy generation in lactic acid bacteria. *J. Bioenerg. Biomembr.* **27**, 467–473 (1995).
- Konings, W. N. Microbial transport: adaptations to natural environments. *Antonie Van Leeuwenhoek* **90**, 325–342 (2006).
- Strahl, H. & Hamoen, L. W. Membrane potential is important for bacterial cell division. *Proc. Natl. Acad. Sci. USA* **107**, 12281–12286 (2010).

12. Schulze, R. J. et al. Membrane protein insertion and proton-motive-force-dependent secretion through the bacterial holo-translocon SecYEG-SecDF-YajC-YidC. *Proc. Natl. Acad. Sci. USA* **111**, 4844–4849 (2014).
13. Prindle, A. et al. Ion channels enable electrical communication in bacterial communities. *Nature* **527**, 59–63 (2015).
14. Yang, C. Y. et al. Encoding membrane-potential-based memory within a microbial community. *Cell Syst.* **10**, 417–423.e413 (2020).
15. Anantharam, V., Allison, M. J. & Maloney, P. C. Oxalate:formate exchange. The basis for energy coupling in *Oxalobacter*. *J. Biol. Chem.* **264**, 7244–7250 (1989).
16. Marty-Teyssset, C. et al. Proton motive force generation by citro-lactic fermentation in *Leuconostoc mesenteroides*. *J. Bacteriol.* **178**, 2178–2185 (1996).
17. Ilgu, H. et al. Insights into the molecular basis for substrate binding and specificity of the wild-type L-arginine/agmatine antiporter AdiC. *Proc. Natl. Acad. Sci. USA* **113**, 10358–10363 (2016).
18. Romano, A., Trip, H., Lonvaud-Funel, A., Lolkema, J. S. & Lucas, P. M. Evidence of two functionally distinct ornithine decarboxylation systems in lactic acid bacteria. *Appl. Environ. Microbiol.* **78**, 1953–1961 (2012).
19. Small, P. L. & Waterman, S. R. Acid stress, anaerobiosis and gadCB: lessons from *Lactococcus lactis* and *Escherichia coli*. *Trends Microbiol.* **6**, 214–216 (1998).
20. Molenaar, D., Bosscher, J. S., ten Brink, B., Driessen, A. J. & Konings, W. N. Generation of a proton motive force by histidine decarboxylation and electrogenic histidine/histamine antiport in *Lactobacillus buchneri*. *J. Bacteriol.* **175**, 2864–2870 (1993).
21. Wolken, W. A., Lucas, P. M., Lonvaud-Funel, A. & Lolkema, J. S. The mechanism of the tyrosine transporter TyrP supports a proton motive tyrosine decarboxylation pathway in *Lactobacillus brevis*. *J. Bacteriol.* **188**, 2198–2206 (2006).
22. Abe, K. et al. Plasmid-encoded asp operon confers a proton motive metabolic cycle catalyzed by an aspartate-alanine exchange reaction. *J. Bacteriol.* **184**, 2906–2913 (2002).
23. Tolner, B., Ubbink-Kok, T., Poolman, B. & Konings, W. N. Cation-selectivity of the L-glutamate transporters of *Escherichia coli*, *Bacillus stearothermophilus* and *Bacillus caldotenax*: dependence on the environment in which the proteins are expressed. *Mol. Microbiol.* **18**, 123–133 (1995).
24. Groeneveld, M., Duurkens, R. & Slotboom D. J. On the mechanism of prokaryotic glutamate transporter homologues - Chapter 5. PhD Thesis thesis, University of Groningen, (2010).
25. Kaback, H. R. & Guan, L. It takes two to tango: the dance of the permease. *J. Gen. Physiol.* **151**, 878–886 (2019).
26. Sobczak, I. & Lolkema, J. S. The 2-hydroxycarboxylate transporter family: physiology, structure, and mechanism. *Microbiol. Mol. Biol. Rev.* **69**, 665–695 (2005).
27. Bandell, M., Ansanay, V., Rachidi, N., Dequin, S. & Lolkema, J. S. Membrane potential-generating malate (MleP) and citrate (CitP) transporters of lactic acid bacteria are homologous proteins. Substrate specificity of the 2-hydroxycarboxylate transporter family. *J. Biol. Chem.* **272**, 18140–18146 (1997).
28. Schulz, P., Garcia-Celma, J. J. & Fendler, K. SSM-based electrophysiology. *Methods* **46**, 97–103 (2008).
29. Bazzone, A., Barthmes, M. & Fendler, K. SSM-based electrophysiology for transporter research. *Methods Enzymol.* **594**, 31–83 (2017).
30. Caspritz, G. & Radler, F. Malolactic enzyme of *Lactobacillus plantarum*. Purification, properties, and distribution among bacteria. *J. Biol. Chem.* **258**, 4907–4910 (1983).
31. Schumann, C. et al. Malolactic enzyme from *Oenococcus oeni*: heterologous expression in *Escherichia coli* and biochemical characterization. *Bioengineered* **4**, 147–152 (2013).
32. Denayrolles, M., Aigle, M. & Lonvaud-Funel, A. Cloning and sequence analysis of the gene encoding *Lactococcus lactis* malolactic enzyme: relationships with malic enzymes. *FEMS Microbiol. Lett.* **116**, 79–86 (1994).
33. Beber, M. E. et al. eQuilibrator 3.0: a database solution for thermodynamic constant estimation. *Nucleic Acids Res.* **50**, D603–D609 (2022).
34. Barreto, J. & Lichtenberger, L. M. Vesicle acidification driven by a millionfold proton gradient: a model for acid influx through gastric cell membranes. *Am. J. Physiol.* **262**, G30–G34 (1992).
35. Waggoner, A. S. The use of cyanine dyes for the determination of membrane potentials in cells, organelles, and vesicles. *Methods Enzymol.* **55**, 689–695 (1979).
36. Ivkova, M. N., Pechatnikov, V. A. & Ivkov, V. G. Mechanism of fluorescent response of the probe diS-C3-(5) to transmembrane potential changes in a lecithin vesicle suspension. *Gen. Physiol. Biophys.* **3**, 97–117 (1984).
37. Fang, G. et al. Manipulation of activity and orientation of membrane-reconstituted di-tripeptide transport protein DtpT of *Lactococcus lactis*. *Mol. Membr. Biol.* **16**, 297–304 (1999).
38. Richard, P., Rigaud, J. L. & Graber, P. Reconstitution of CF0F1 into liposomes using a new reconstitution procedure. *Eur. J. Biochem.* **193**, 921–925 (1990).
39. Bailoni, E. & Poolman, B. ATP recycling fuels sustainable glycerol 3-phosphate formation in synthetic cells fed by dynamic dialysis. *ACS Synth. Biol.* **11**, 2348–2360 (2022).
40. Driessen, A. J., van Leeuwen, C. & Konings, W. N. Transport of basic amino acids by membrane vesicles of *Lactococcus lactis*. *J. Bacteriol.* **171**, 1453–1458 (1989).
41. Fang, G., Konings, W. N. & Poolman, B. Kinetics and substrate specificity of membrane-reconstituted peptide transporter DtpT of *Lactococcus lactis*. *J. Bacteriol.* **182**, 2530–2535 (2000).
42. Viitanen, P., Newman, M. J., Foster, D. L., Wilson, T. H. & Kaback, H. R. Purification, reconstitution, and characterization of the lac permease of *Escherichia coli*. *Methods Enzymol.* **125**, 429–452 (1986).
43. Gaiko, O., Bazzone, A., Fendler, K. & Kaback, H. R. Electrophysiological characterization of uncoupled mutants of LacY. *Biochemistry* **52**, 8261–8266 (2013).
44. Lopez Mora, N. et al. The membrane transporter lactose permease increases lipid bilayer bending rigidity. *Biophys. J.* **120**, 3787–3794 (2021).
45. Olsen, S. G. & Brooker, R. J. Analysis of the structural specificity of the lactose permease toward sugars. *J. Biol. Chem.* **264**, 15982–15987 (1989).
46. Guan, L. & Kaback, H. R. Binding affinity of lactose permease is not altered by the H<sup>+</sup> electrochemical gradient. *Proc. Natl. Acad. Sci. USA* **101**, 12148–12152 (2004).
47. Tavoulari, S. & Frillingos, S. Substrate selectivity of the melibiose permease (MelY) from *Enterobacter cloacae*. *J. Mol. Biol.* **376**, 681–693 (2008).
48. Veenhoff, L. M. & Poolman, B. Substrate recognition at the cytoplasmic and extracellular binding site of the lactose transport protein of *Streptococcus thermophilus*. *J. Biol. Chem.* **274**, 33244–33250 (1999).
49. Noireaux, V. & Libchaber, A. A vesicle bioreactor as a step toward an artificial cell assembly. *Proc. Natl. Acad. Sci. USA* **101**, 17669–17674 (2004).
50. Krishnan, S. et al. Molecular transport through large-diameter DNA nanopores. *Nat. Commun.* **7**, 12787 (2016).
51. Fragasso, A. et al. Reconstitution of ultrawide DNA origami pores in liposomes for transmembrane transport of macromolecules. *ACS Nano* **15**, 12768–12779 (2021).
52. Garamella, J., Majumder, S., Liu, A. P. & Noireaux, V. An adaptive synthetic cell based on mechanosensing, biosensing, and inducible gene circuits. *ACS Synth. Biol.* **8**, 1913–1920 (2019).

53. Gaut, N. J. & Adamala, K. P. Reconstituting natural cell elements in synthetic cells. *Adv. Biol. (Weinh.)* **5**, e2000188 (2021).
54. Bailoni, E. et al. Minimal out-of-equilibrium metabolism for synthetic cells: a membrane perspective. *ACS Synth. Biol.* **12**, 922–946 (2023).
55. Kim, J. W. et al. Structural insights into the elevator-like mechanism of the sodium/citrate symporter CitS. *Sci. Rep.* **7**, 2548 (2017).
56. Bandell, M. & Lolkema, J. S. Stereoselectivity of the membrane potential-generating citrate and malate transporters of lactic acid bacteria. *Biochemistry* **38**, 10352–10360 (1999).
57. Drew, D. & Boudker, O. Shared molecular mechanisms of membrane transporters. *Annu. Rev. Biochem.* **85**, 543–572 (2016).
58. Jardetzky, O. Simple allosteric model for membrane pumps. *Nature* **211**, 969–970 (1966).
59. Lee, K. Y. et al. Photosynthetic artificial organelles sustain and control ATP-dependent reactions in a protocellular system. *Nat. Biotechnol.* **36**, 530–535 (2018).
60. Berhanu, S., Ueda, T. & Kuruma, Y. Artificial photosynthetic cell producing energy for protein synthesis. *Nat. Commun.* **10**, 1325 (2019).
61. Biner, O., Fedor, J. G., Yin, Z. & Hirst, J. Bottom-up construction of a minimal system for cellular respiration and energy regeneration. *ACS Synth. Biol.* **9**, 1450–1459 (2020).
62. Uzdavinyis, P. et al. Dissecting the proton transport pathway in electrogenic Na<sup>+</sup>/H<sup>+</sup> antiporters. *Proc. Natl. Acad. Sci. USA* **114**, E1101–E1110 (2017).
63. Ge, T. et al. The role of the pentose phosphate pathway in diabetes and cancer. *Front. Endocrinol. (Lausanne)* **11**, 365 (2020).
64. Partipilo, M. et al. Minimal pathway for the regeneration of redox cofactors. *JACS Au* **1**, 2280–2293 (2021).
65. Pols, T. et al. A synthetic metabolic network for physicochemical homeostasis. *Nat. Commun.* **10**, 4239 (2019).
66. Deamer, D. W. Proton permeation of lipid bilayers. *J. Bioenerg. Biomembr.* **19**, 457–479 (1987).
67. Redelmeier, T. E., Mayer, L. D., Wong, K. F., Bally, M. B. & Cullis, P. R. Proton flux in large unilamellar vesicles in response to membrane potentials and pH gradients. *Biophys. J.* **56**, 385–393 (1989).
68. Rossignol, M., Thomas, P. & Grignon, C. Proton permeability of liposomes from natural phospholipid mixtures. *Biochim. Biophys. Acta* **684**, 195–199 (1982).
69. Krulwich, T. A., Sachs, G. & Padan, E. Molecular aspects of bacterial pH sensing and homeostasis. *Nat. Rev. Microbiol.* **9**, 330–343 (2011).
70. Biquet-Bisquert, A. et al. Spatio-temporal dynamics of the proton motive force on single bacterial cells. *bioRxiv*, <https://doi.org/10.1101/2023.04.03.535353> (2023).
71. Kashket, E. R. The proton motive force in bacteria: a critical assessment of methods. *Annu. Rev. Microbiol.* **39**, 219–242 (1985).
72. Lolkema, J. S. & Poolman, B. Uncoupling in secondary transport proteins. A mechanistic explanation for mutants of lac permease with an uncoupled phenotype. *J. Biol. Chem.* **270**, 12670–12676 (1995).
73. Poolman, B., Knol, J. & Lolkema, J. S. Kinetic analysis of lactose and proton coupling in Glu379 mutants of the lactose transport protein of *Streptococcus thermophilus*. *J. Biol. Chem.* **270**, 12995–13003 (1995).
74. Yue, K. et al. Bottom-up synthetic biology using cell-free protein synthesis. *Adv. Biochem. Eng. Biotechnol.* **185**, 1–20 (2023).
75. Gonzales, D. T., Suraritdechachai, S. & Tang, T. D. Compartmentalized cell-free expression systems for building synthetic cells. *Adv. Biochem. Eng. Biotechnol.* **186**, 77–101 (2023).
76. Garenne, D. et al. Cell-free gene expression. *Nat. Rev. Methods Prim.* **1**, 49 (2021).
77. Jewett, M. C., Calhoun, K. A., Voloshin, A., Wu, J. J. & Swartz, J. R. An integrated cell-free metabolic platform for protein production and synthetic biology. *Mol. Syst. Biol.* **4**, 220 (2008).
78. Cai, Q. et al. A simplified and robust protocol for immunoglobulin expression in *Escherichia coli* cell-free protein synthesis systems. *Biotechnol. Prog.* **31**, 823–831 (2015).
79. Holden, H. M., Rayment, I. & Thoden, J. B. Structure and function of enzymes of the Leloir pathway for galactose metabolism. *J. Biol. Chem.* **278**, 43885–43888 (2003).
80. Varela, M. F. & Wilson, T. H. Molecular biology of the lactose carrier of *Escherichia coli*. *Biochim Biophys. Acta* **1276**, 21–34 (1996).
81. Henderson, R. K., Fendler, K. & Poolman, B. Coupling efficiency of secondary active transporters. *Curr. Opin. Biotechnol.* **58**, 62–71 (2019).
82. Nelson, N., Sacher, A. & Nelson, H. The significance of molecular slips in transport systems. *Nat. Rev. Mol. Cell Biol.* **3**, 876–881 (2002).
83. Hagting, A., Kunji, E. R., Leenhouts, K. J., Poolman, B. & Konings, W. N. The di- and tripeptide transport protein of *Lactococcus lactis*. A new type of bacterial peptide transporter. *J. Biol. Chem.* **269**, 11391–11399 (1994).
84. Garai, P., Chandra, K. & Chakravorty, D. Bacterial peptide transporters: Messengers of nutrition to virulence. *Virulence* **8**, 297–309 (2017).
85. de Koning, H. P., Watson, C. J. & Jarvis, S. M. Characterization of a nucleoside/proton symporter in procyclic *Trypanosoma brucei*. *J. Biol. Chem.* **273**, 9486–9494 (1998).
86. Haferkamp, I. et al. Tapping the nucleotide pool of the host: novel nucleotide carrier proteins of *Protochlamydia amoebophila*. *Mol. Microbiol.* **60**, 1534–1545 (2006).
87. Geertsma, E. R. & Poolman, B. High-throughput cloning and expression in recalcitrant bacteria. *Nat. Methods* **4**, 705–707 (2007).
88. Newman, M. J. & Wilson, T. H. Solubilization and reconstitution of the lactose transport system from *Escherichia coli*. *J. Biol. Chem.* **255**, 10583–10586 (1980).
89. Geertsma, E. R., Nik Mahmood, N. A., Schuurman-Wolters, G. K. & Poolman, B. Membrane reconstitution of ABC transporters and assays of translocator function. *Nat. Protoc.* **3**, 256–266 (2008).
90. Clement, N. R. & Gould, J. M. Pyranine (8-hydroxy-1,3,6-pyrenetrissulfonate) as a probe of internal aqueous hydrogen ion concentration in phospholipid vesicles. *Biochemistry* **20**, 1534–1538 (1981).
91. Pellegrini, D., Onor, M., Degano, I. & Bramanti, E. Development and validation of a novel derivatization method for the determination of lactate in urine and saliva by liquid chromatography with UV and fluorescence detection. *Talanta* **130**, 280–287 (2014).
92. Bazzone, A., Madej, M. G., Kaback, H. R. & Fendler, K. pH regulation of electrogenic sugar/H<sup>+</sup> symport in MFS sugar permeases. *PLoS One* **11**, e0156392 (2016).
93. Gendreau, S. et al. A trimeric quaternary structure is conserved in bacterial and human glutamate transporters. *J. Biol. Chem.* **279**, 39505–39512 (2004).
94. Juers, D. H., Matthews, B. W. & Huber, R. E. LacZ beta-galactosidase: structure and function of an enzyme of historical and molecular biological importance. *Protein Sci.* **21**, 1792–1807 (2012).
95. Morales, F. C. & Bianconi, M. L. Influence of the oligomeric state of yeast hexokinase isozymes on inactivation and unfolding by urea. *Biophys. Chem.* **91**, 183–190 (2001).
96. Saliola, M. et al. Intracellular NADPH levels affect the oligomeric state of the glucose 6-phosphate dehydrogenase. *Eukaryot. Cell* **11**, 1503–1511 (2012).

## Acknowledgements

The authors thank Gea Schuurman-Wolters for assistance with the expression and purification of LacY, Ineke van't Land-Kuper for the preparation of *E. coli* polar lipids extract, and Marc C. A. Stuart for providing assistance with the cryo-TEM analysis of vesicles. The research was funded by the NWO Gravitation program “Building a synthetic cell”

(BaSyC) and by the European Union's Horizon 2020 research and innovation program under the Marie Skłodowska-Curie grant agreement no.: 860954.

### Author contributions

M.P.R. performed the SSM measurements, analysis of enzymatic decarboxylation reaction in solution, pH, and membrane potential determination in the vesicles. M.P.R. and Z.R.A. performed the uptake of radiolabeled substrates and fluorescence measurements. B.G. cloned and expressed the *mleS* and *mleP* genes and performed the radiolabel transport experiments with MleP. M.P.R., Z.R.A., B.G., D.J.S., and B.P. designed the research and analyzed the data. M.P.R., Z.R.A., D.J.S., and B.P. wrote the paper. D.J.S. and B.P. supervised the research.

### Competing interests

The authors declare no competing interests.

### Additional information

**Supplementary information** The online version contains supplementary material available at <https://doi.org/10.1038/s41467-024-52085-z>.

**Correspondence** and requests for materials should be addressed to Bert Poolman.

**Peer review information** *Nature Communications* thanks Kwanwoo Shin and the other, anonymous, reviewers for their contribution to the peer review of this work. A peer review file is available.

**Reprints and permissions information** is available at <http://www.nature.com/reprints>

**Publisher's note** Springer Nature remains neutral with regard to jurisdictional claims in published maps and institutional affiliations.

**Open Access** This article is licensed under a Creative Commons Attribution-NonCommercial-NoDerivatives 4.0 International License, which permits any non-commercial use, sharing, distribution and reproduction in any medium or format, as long as you give appropriate credit to the original author(s) and the source, provide a link to the Creative Commons licence, and indicate if you modified the licensed material. You do not have permission under this licence to share adapted material derived from this article or parts of it. The images or other third party material in this article are included in the article's Creative Commons licence, unless indicated otherwise in a credit line to the material. If material is not included in the article's Creative Commons licence and your intended use is not permitted by statutory regulation or exceeds the permitted use, you will need to obtain permission directly from the copyright holder. To view a copy of this licence, visit <http://creativecommons.org/licenses/by-nc-nd/4.0/>.

© The Author(s) 2024